Core-Collapse Supernovae

— Reflections and Directions —

Hans-Thomas Janka[1],
Florian Hanke[1], Lorenz Hüdepohl[1], Andreas Marek[1],
Bernhard Müller[1], and Martin Obergaulinger[2]

[1]*Max Planck Institute for Astrophysics, Karl-Schwarzschild-Str. 1, 85748 Garching, Germany*
[2]*Departament d´Astronomia i Astrofísica, Universitat de València, Edifici d´Investigació Jeroni Muñoz, C/ Dr. Moliner, 50, E-46100 Burjassot (València), Spain*

Core-collapse supernovae are among the most fascinating phenomena in astrophysics and provide a formidable challenge for theoretical investigation. They mark the spectacular end of the lives of massive stars and, in an explosive eruption, release as much energy as the sun produces during its whole life. A better understanding of the astrophysical role of supernovae as birth sites of neutron stars, black holes, and heavy chemical elements, and more reliable predictions of the observable signals from stellar death events are tightly linked to the solution of the long-standing puzzle how collapsing stars achieve to explode. In this article our current knowledge of the processes that contribute to the success of the explosion mechanism are concisely reviewed. After a short overview of the sequence of stages of stellar core-collapse events, the general properties of the progenitor-dependent neutrino emission will be briefly described. Applying sophisticated neutrino transport in axisymmetric (2D) simulations with general relativity as well as in simulations with an approximate treatment of relativistic effects, we could find successful neutrino-driven explosions for a growing set of progenitor stars. First results of three-dimensional (3D) models have been obtained, and magnetohydrodynamic simulations demonstrate that strong initial magnetic fields in the pre-collapse core can foster the onset of neutrino-powered supernova explosions even in nonrotating stars. These results are discussed in the context of the present controversy about the value of 2D simulations for exploring the supernova mechanism in realistic 3D environments, and they are interpreted against the background of the current disagreement on the question whether the standing accretion shock instability (SASI) or neutrino-driven convection is the crucial agency that supports the onset of the explosion.

Subject Index: 483, 421, 423, 415, 451, 452, 242

§1. Supernova theory in a nutshell

Massive stars in the range between $\sim 8\,M_\odot$ and several $10\,M_\odot$ develop low-entropy cores, in which relativistic electrons dominate the pressure. Heavy nuclei yield only a small, though important, contribution to providing stabilization against the inward pull of gravity. The core consists of the final products of the star's nuclear burning history. It is surrounded by concentric shells that, from outside inward, contain the successively heavier ashes of all previous burning stages (Fig. 1).

Shell burning leads to a continuous growth of the mass of the central core until gravitational instability finally sets in. At this time the core resembles a hot white dwarf close to its maximum mass of the order of the Chandrasekhar mass. It has

a typical diameter of about 3000 km, a central temperature around 10^{10} K (or approximately 1 MeV), a central density of several $10^9\,\mathrm{g\,cm^{-3}}$, an entropy of ∼0.7 to ∼1 k_B per nucleon (k_B is Boltzmann's constant), and a proton-to-baryon ratio of around 0.45. The accelerating contraction and ultimately the collapse of the degenerate core is initiated by the shift of nuclear statistical equilibrium (NSE). As the temperature in the contracting core increases, high-energy photons produce a growing number of α particles and free nucleons. Thermal energy is thus consumed to overcome the binding energy of heavy nuclei. This endothermic process, which partially disintegrates the iron-group material that had been assembled during the final burning stage of the progenitor, lowers the effective adiabatic index*) below the critical value (≈4/3) for gravitational instability. With growing density, electron captures on heavy nuclei and on free protons become more and more important. The corresponding loss of lepton number by the production and escape of electron neutrinos softens the pressure increase with density even further and accelerates the collapse (Fig. 2, top left panel).

Neutrinos become trapped in the collapsing matter at a density of roughly $10^{12}\,\mathrm{g\,cm^{-3}}$, at which conditions their diffusion timescale out of the core begins to exceed the freefall timescale of the gas. Despite neutrino trapping, the collapse cannot be stopped before nuclear matter density (∼$2.7 \times 10^{14}\,\mathrm{g\,cm^{-3}}$) is reached and the equation of state stiffens because of repulsive contributions to the nucleon interaction potential. When the homologously and subsonically collapsing inner core decelerates and rebounds into the surrounding, supersonically infalling layers, sound waves steepen into a shock front (Fig. 2, top right panel). This shock front expands into the overlying Fe-core material, but is quickly damped by energy losses due to the dissociation of Fe-group nuclei into free nucleons, which extracts a thermal energy of about 8.8 MeV per nucleon from the postshock matter. Only 1–2 ms after shock formation, the velocities downstream of the shock have thus become negative. Nevertheless, the shock continues to propagate outward in mass

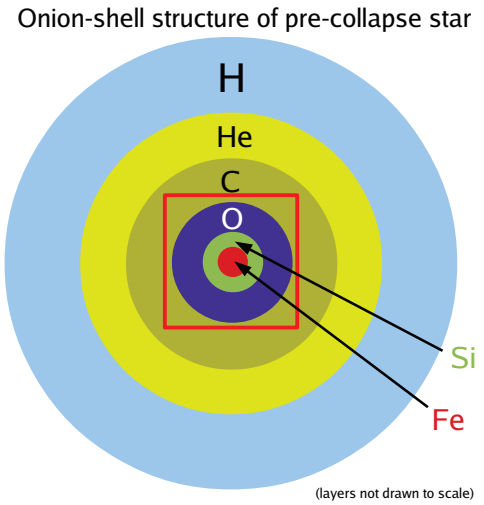

Fig. 1. Schematic onion-shell structure of a supernova progenitor star before core collapse. Only the main elemental constituents of the different composition shells, which contain the products and ashes of the sequence of nuclear burning stages, are indicated. Note that the radial thickness of the layers is not drawn to scale. The red square indicates the inner region zoomed into in Fig. 2.

*) The effective (dynamically relevant) adiabatic index is defined as the logarithmic density derivative of the pressure, $(\partial \ln P/\partial \ln \rho)_m$, along a fluid element's trajectory, averaged over the volume of the collapsing core. It governs the transition to gravitational instability and the collapse dynamics.[1)]

and radius because initially the high mass accretion rate of up to several solar masses per second leads to the accumulation of a thick layer of dense matter behind the shock. Only when the mass accretion rate has decayed sufficiently and the hot, bloated mantle of the proton-neutron star begins to shrink in response to the lepton number and energy loss through neutrinos, the radial shock expansion comes to a halt and the shock forms a stagnant accretion shock at a radius between 100 and 200 km (Fig. 2, middle left panel). Quasi-stationary conditions apply later on with only slow changes of the mass accretion rate, $\dot{M}$, neutron star mass $M_{\rm ns}$ and radius $R_{\rm ns}$, and neutrino emission parameters (luminosity L_ν and mean spectral energy $\langle\epsilon_\nu\rangle$). In nonexploding spherically symmetric (i.e., one-dimensional, 1D) simulations the shock retreats and its radius follows the contraction of the nascent neutron star roughly according to the relation.[2)]

$$R_{\rm s} \propto \frac{(L_\nu \langle\epsilon_\nu^2\rangle)^{4/9} R_{\rm ns}^{16/9}}{\dot{M}^{2/3} M_{\rm ns}^{1/3}} \,. \qquad (1\cdot1)$$

High mass accretion rates therefore tend to damp the shock expansion while neutrino-energy deposition behind the shock, which depends on the product $L_\nu \langle\epsilon_\nu^2\rangle$[*)], can drive shock expansion. This issue will be elaborated on further below.

In order to successfully launch a supernova explosion, some mechanism is necessary by which the stalled shock can be revived. Such a mechanism needs to tap the huge reservoir of gravitational binding energy that is released during the formation of a neutron star. During the infall of the stellar core the energy is first converted to internal energy by hydrodynamic forces (i.e., compression and the viscous dissipation of kinetic energy in matter decelerated in the accretion shock). The degeneracy and thermal energy of electrons and nucleons thus stored in the proto-neutron is subsequently radiated away by neutrinos over a timescale of many seconds.

Deep in the highly degenerate neutron-star interior electron neutrinos, ν_e, are first produced by electron captures on protons. On their diffusive propagation towards the neutrinosphere, these electron neutrinos lose some of their energy in absorption-reemission processes as well as in scattering reactions with electrons and free neutrons and protons (Fig. 3). This effect together with the gravitational settling and compression of the outer layers of the proto-neutron star initially leads to rising temperatures before after some seconds cooling sets in. Since the degeneracy is partially lifted in the hot proto-neutron star mantle, the secondary production of electron antineutrinos, $\bar{\nu}_e$, by positron captures on neutrons becomes possible. Neutrino-antineutrino pairs of all three flavors are created by thermal processes, i.e., nucleon-nucleon bremsstrahlung and electron-positron annihilation. Pure neutrino reactions (Fig. 3) also contribute to the shaping of the emitted spectra of muon and tau neutrinos and antineutrinos (ν_μ, $\bar{\nu}_\mu$, ν_τ, $\bar{\nu}_\tau$),[3)] which are not produced by fast beta reactions and thus are less tightly coupled to the stellar medium.

Even a small fraction of the huge energy reservoir of several 10^{53} ergs carried

[*)] The energy transfer by neutrinos scales linearly with the neutrino luminosity and the average interaction cross section. The latter increases roughly with the luminosity-averaged square of the neutrino energy.

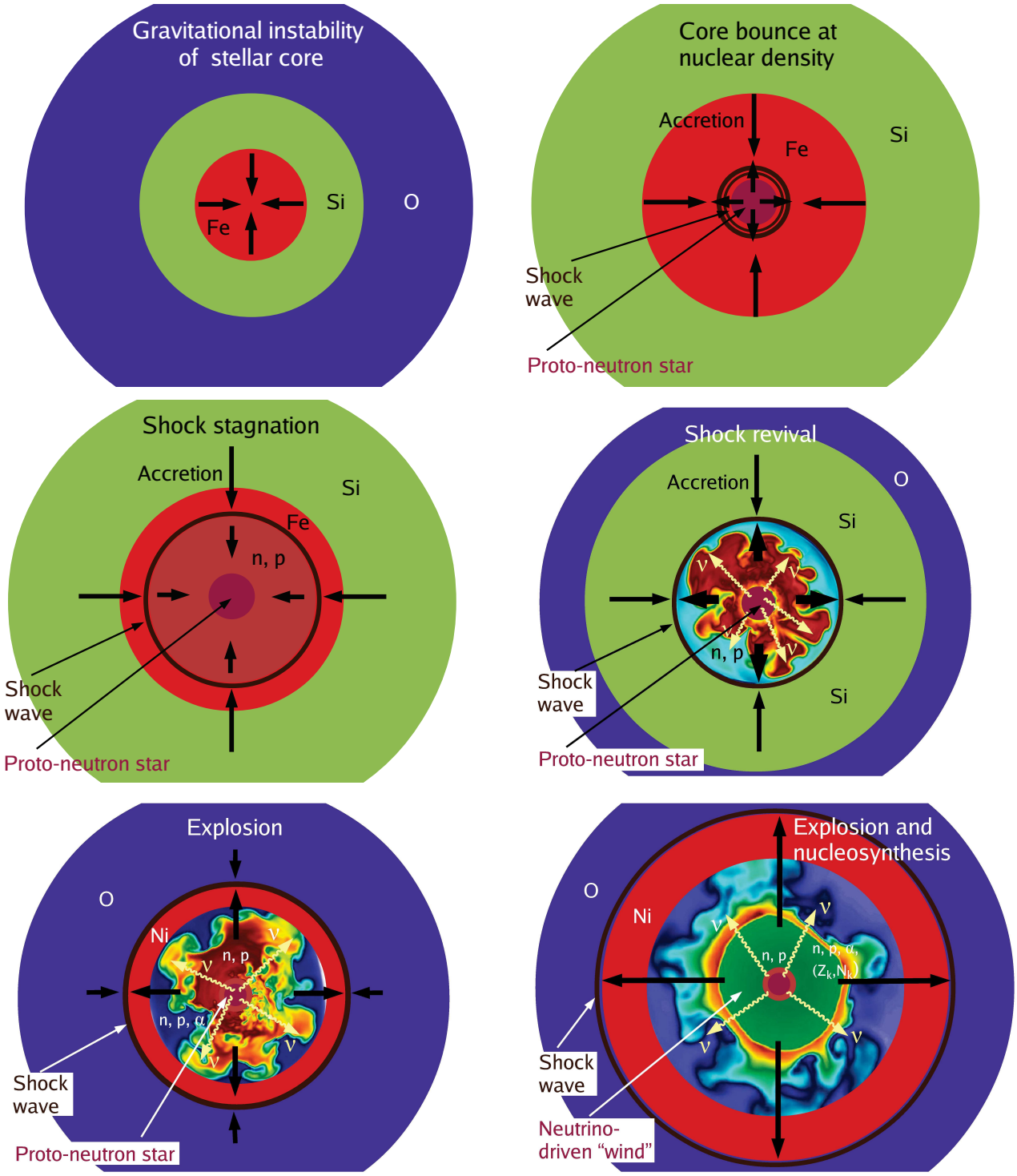

Fig. 2. Schematic representation of the evolution stages from the onset of stellar core collapse (*top left*) to the development of a supernova explosion on a scale of several 1000 kilometers. The displayed intermediate stages show the moment of core bounce and shock formation (*top right*), shock stagnation and onset of quasi-stationary accretion (*middle left*), beginning of the reexpansion of the shock wave ("shock revival", *middle right*), and acceleration of the explosion (*bottom left*). Nickel formation is indicated in the matter heated by the outgoing shock, but also the rising bubbles of neutrino-heated ejecta and the essentially spherically symmetric neutrino-driven wind (*bottom right*) are interesting sites for nucleosynthesis.

away by neutrinos is already sufficient to account for the canonical explosion energy of a core-collapse supernova, which ranges between some 10^{50} erg to around 10^{51} erg. It may appear astonishing that the explosion selects an energy scale that is 2–3 orders of magnitude lower than the reservoir of available energy. The energy scale of the explosion, however, is not set by the neutron star binding energy but by the structure of the progenitor configuration. The degenerate iron core closely resembles a white dwarf, embedded in the more or less dense stratification of concentric stellar shells containing lighter nuclear burning products. The energy scale of the explosion is determined by the binding energy of the progenitor layers in immediate vicinity of the initial mass cut between proto-neutron star and supernova ejecta*). For typical progenitor stars the binding energy of the silicon shell and overlying layers is of the order of 10^{50}–10^{51} ergs, similar to the binding energy of the pre-collapse Fe core. Any self-regulated mechanism will tend to deposit an energy of this magnitude: Once matter has received this amount of energy, it will tend to become unbound and will expand away from what is going to become the bifurcation region between compact remnant and supernova ejecta.

The *delayed neutrino-driven explosion mechanism*[7] is such a self-regulated process, because after absorbing energy in interactions with neutrinos, the heated matter expands away from the neutrino-heating region. This naturally limits the energy input. Neutrinos are produced in huge numbers in the dense and very hot interior of the nascent neutron star and leave the neutrinospheric region with roughly blackbody spectra and temperatures of typically 3–6 MeV. This is considerably hotter than the gas in the layer between neutrinosphere and stalled shock. Neutrino heating and cooling in this region is dominated by the absorption of electron neutrinos and antineutrinos on free neutrons and protons and the inverse of these processes,

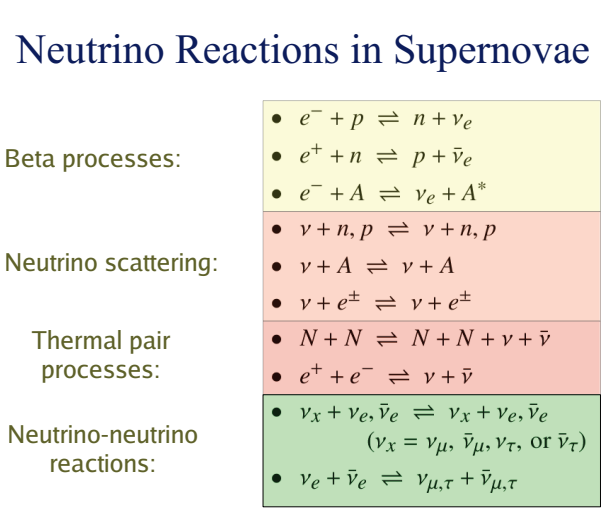

Fig. 3. Summary of important neutrino reactions in the supernova core and/or nascent neutron star.[4)–6)] The symbol ν can mean any type of neutrino, A represents an atomic nucleus, and N means neutron (n) or proton (p).

$$\nu_e + n \longleftrightarrow p + e^- \,, \tag{1·2}$$

$$\bar{\nu}_e + p \longleftrightarrow n + e^+ \,. \tag{1·3}$$

The corresponding rates per nucleon q_ν^+ and q_ν^- for the energy input and loss of the

*) Note that the collapse roughly conserves the total energy of the infalling shells so that the energetic considerations are possible for the progenitor conditions.

stellar medium are approximately given by:[8)]

$$q^{+}_{\nu_e+\bar{\nu}_e} \approx 160\ \frac{L_\nu}{10^{52}\,\mathrm{erg/s}} \left(\frac{r}{100\,\mathrm{km}}\right)^{-2} \left(\frac{k_\mathrm{B}T_\nu}{4\,\mathrm{MeV}}\right)^{2}\ \mathrm{MeV\,s^{-1}}\ \text{per nucleon}, \quad (1{\cdot}4)$$

$$q^{-}_{\nu_e+\bar{\nu}_e} \approx 145\ \left(\frac{k_\mathrm{B}T_\nu}{2\,\mathrm{MeV}}\right)^{6}\ \mathrm{MeV\,s^{-1}}\ \text{per nucleon}. \quad (1{\cdot}5)$$

Here L_ν and T_ν are the luminosity and spectral temperature of either ν_e or $\bar{\nu}_e$ (whose emission characteristics during the shock revival phase are similar), the squared radius r measures the geometric dilution of the flux leaving the neutrinosphere, and $T(r)$ is the local gas temperature. The heating and cooling rates in Eqs. (1·4) and (1·5) have roughly the same magnitude. This means that both processes are in tight competition. Indeed, the neutrinosphere is surrounded by a cooling layer, in which neutrino losses dominate. Since, however, the temperature declines roughly like r^{-1}, the cooling rate falls off with r^{-6} and therefore much steeper than the heating rate, which follows basically an r^{-2} dependence. Consequently, there must be a "gain radius" R_g, outside of which neutrino heating becomes stronger than neutrino cooling.[7)]

Neutrinos can deposit considerable amounts of energy in the layer between R_g and the shock position at radius R_s, where most of the nuclei are dissociated into free nucleons (the preheating in the rapidly infalling, undissociated material ahead of the shock is small). The optical depth for ν_e and $\bar{\nu}_e$ absorption in the gain layer between R_g and R_s can be estimated to be[2)]

$$\tau_\mathrm{gain} \approx 0.026 \left(\frac{k_\mathrm{B}T_\nu}{4\,\mathrm{MeV}}\right)^{2} \left(\frac{\dot{M}}{0.1\,M_\odot/\mathrm{s}}\right) \left(\frac{R_\mathrm{s}}{200\,\mathrm{km}}\right)^{3/2} \left(\frac{R_\mathrm{g}}{100\,\mathrm{km}}\right)^{-2} \left(\frac{M_\mathrm{ns}}{1.5\,M_\odot}\right)^{-1/2}, \quad (1{\cdot}6)$$

where $\dot{M}$ and M_ns are again the rate of mass accretion by the shock and the neutron star mass, respectively. For typical mass accretion rates of $\sim$0.1–0.3 $M_\odot\,\mathrm{s^{-1}}$ and neutrino spectral temperatures $k_\mathrm{B}T_\nu \approx 4$–6 MeV the optical depth is 0.05–0.1, which means that up to about 10% of the through-going neutrinos can be captured by a neutron or proton.

If the neutrino energy deposition is sufficiently strong, the stalled shock can be revived to potentially initiate a successful supernova explosion (Fig. 2, middle right panel). The threshold for runaway conditions can be coined in terms of a critical luminosity,[9)] $L_{\nu,\mathrm{c}}(\dot{M})$ (for $\nu = \nu_e$ or $\bar{\nu}_e$), which depends on the mass accretion rate of the shock. A steady accretion shock cannot be maintained when the neutrino luminosity exceeds this critical value (for a very detailed analysis, see Ref. 10)). The threshold value increases with higher $\dot{M}$, because neutrino heating has to overcome the higher ram pressure of the infalling material. Due to its stronger gravity also a larger neutron star mass M_ns requires a higher neutrino luminosity for shock revival. The dependence of $L_{\nu,\mathrm{c}}$ on $\dot{M}$ and M_ns can be analytically estimated on grounds of simple considerations. Shock expansion can become strong when neutrinos heat the postshock matter faster than it can be advected with the accretion flow from the shock downward through the gain radius into the cooling layer, where the gas loses

its energy by neutrino emission.[11)–13)] This requirement is confirmed by all existing numerical simulations (e.g., 13)–18)). Thus requiring the neutrino-heating timescale to be shorter than the advection timescale through the gain layer one obtains for the critical luminosity:[2)]

$$L_{\nu,\mathrm{c}}(\dot{M}) \propto \beta^{-2/5}\, \dot{M}^{2/5}\, M_{\mathrm{ns}}^{4/5}\,, \tag{1·7}$$

where β parametrizes the ratio of postshock density to preshock density[*)]. This functional dependence nicely fits the critical curves obtained in Ref. 9), but it predicts considerably steeper power-law dependences on M_{ns} and $\dot{M}$ than the critical explosion condition of Eq. (11) in Ref. 18). It should be noted, however, that in the latter reference the optical depth was used as a constant free fit parameter but should actually be expressed as function of the fundamental quantities (M_{ns}, $\dot{M}$) that govern the overall dynamics and structure of the postshock layer.

Convective overturn in the neutrino-heating region has been recognized to support the onset of the explosion[19)–21)] and to lower the critical luminosity.[14),21)–24)] Nonradial and partially turbulent mass motions do not only stretch the dwell time of matter in the gain layer. Convective downdrafts carry postshock material to the immediate vicinity of the gain radius, where neutrino heating is strongest. Moreover, the outward rise and expansion cooling of neutrino-heated gas in buoyant high-entropy bubbles reduce the energy loss by reemission of neutrinos and push the shock farther out. The residency time of matter in the gain layer is thus prolonged even more. This combination of favorable circumstances is crucial for the development of runaway conditions. Nonradial oscillations and sloshing motions of the shock, which are associated with the growth of the **s**tanding **a**ccretion **s**hock **i**nstability (SASI[25)]), seem to have a similarly favorable influence on the conditions for neutrino-driven explosions.[15)–17),26)] All these effects reduce the critical value of the neutrino luminosity in multi-dimensional models compared to the 1D case.[14),18),21),23),24)]

When the blast wave takes off, explosive burning leads to the production of ^{56}Ni and other radioactive species in the shock-heated silicon and/or oxygen layers (Fig. 2, bottom left panel). Recombination of nucleons to alpha particles and Fe-group nuclei in the neutrino-heated high-entropy plumes contributes to the nucleosynthetic yields, and the neutrino-driven baryonic outflow ("neutrino wind"), which is shed off the surface of the nascent neutron star by neutrino heating to fill the surroundings of the compact remnant after accretion has ended (Fig. 2, bottom right panel), is considered as an interesting site for the formation of trans-iron nuclei up to $A \sim 110$ in a weak r-process and of p-rich isotopes in the neutrino-proton process, depending on whether the wind develops a neutron or proton excess (for a review, see Ref. 27)). Both the electron fraction, Y_e, and the entropy in the early neutrino-heated ejecta and in the neutrino-driven wind have a crucial influence on the nucleosynthesis, and both are set by the neutrino interactions of Eqs. (1·2) and (1·3). Therefore they depend sensitively on the emission properties (luminosities and spectra) of the ν_e and $\bar{\nu}_e$ radiated by the forming neutron star and on the expansion dynamics of the ejecta (which determines the time interval of intense neutrino interactions). Also

[*)] The numerical factor in the scaling relation is found to be $\sim$(5–6)$\times 10^{52}$ erg/s for $\beta \sim 10$, $\dot{M} = 1\,M_\odot$/s, and $M_{\mathrm{ns}} = 1.5\,M_\odot$.

neutrino oscillations, in particular collective neutrino flavor transformations, can have an impact on the neutron-to-proton ratio that develops in the ejecta on their way away from the neutrino source (e.g., Ref. 28)).

It should be noted that the explosion energy of the supernova is *not* determined at the instant when the explosion sets in; in particular it is not given by the energy neutrinos have transferred to the postshock matter up to this time. Instead, the total energy (i.e., internal plus gravitational plus the initially much smaller kinetic energy) of the gain layer is close to zero when the shock begins to propagate outward, which means that this layer is only marginally unbound.[8),10)] This is observed in all numerical models of neutrino-driven explosions (e.g., 15), 16), 29)). Instead, the explosion energy builds up only on a longer timescale of several 100 ms to more than a second. There are several sources that contribute to the final explosion energy (see results and discussions in Refs. 15), 29), 30)). First, neutrinos continue to heat "cool" gas that is freshly accreted through the shock and channelled towards the gain radius in convective downdrafts to replace there the hot matter that expands in high-entropy bubbles driving the shock expansion.[15)] In addition, the recombination of free nucleons to α particles and heavy nuclei in the ejecta releases up to $\sim$9 MeV per nucleon and is a very efficient source of energy for the developing explosion ($0.1\,M_\odot$ of nucleonic matter can provide up to about 1.7×10^{51} erg of recombination energy) as pointed out in Ref. 29). It should be noted that the production of free nucleons by nuclear photodisintegration in the infalling matter —either when the gas passes the accretion shock or when it is compressed and neutrino heated in the accretion downflows— mostly taps the gravitational binding energy and only to a smaller extent is fuelled by neutrino absorption. The conversion of gravitational binding energy to nuclear photodisintegration energy during the infall is therefore an important energy storage whose contents are released when the matter is subsequently reejected and cools in the explosive outflow. Similarly, the neutrino-driven wind blown off the hot neutron star's surface gains power from neutrino heating as well as nuclear recombination. Its energy can yield a significant contribution to the energy budget of the supernova explosion. Scheck et al.[29)] found that $\sim$30–70% of the blast-wave energy can be provided by this long-term outflow from the proto-neutron star (with higher relative importance for stronger explosions). In contrast, nuclear burning of silicon and oxygen to nickel in the shock-heated outer layers yields only a smaller amount of extra energy for the supernova; the production of $0.1\,M_\odot$ of iron-group material (a typical number for normal core-collapse supernovae) releases only about 10^{50} erg. During the first $\sim$1–3 s seconds of the explosion all these energy souces have to provide enough energy to unbind the overlying stellar layers (whose binding energy can range between $\lesssim 10^{50}$ erg and about 10^{51} erg, depending on the core mass and compactness of the progenitor star) and, beyond that, to account for the measurable kinetic energy of the supernova. If the blast-wave energy is too low, some of the matter swept up by the outgoing shock will not be able to escape to infinity and will fall back onto the compact remnant. Because much or even most of the nucleosynthesized ^{56}Ni may thus be accreted instead of being expelled, such fallback supernovae are expected to be faint and hard to observe. It is therefore empirically unclear which fraction of stellar core collapses might belong to such types of events.

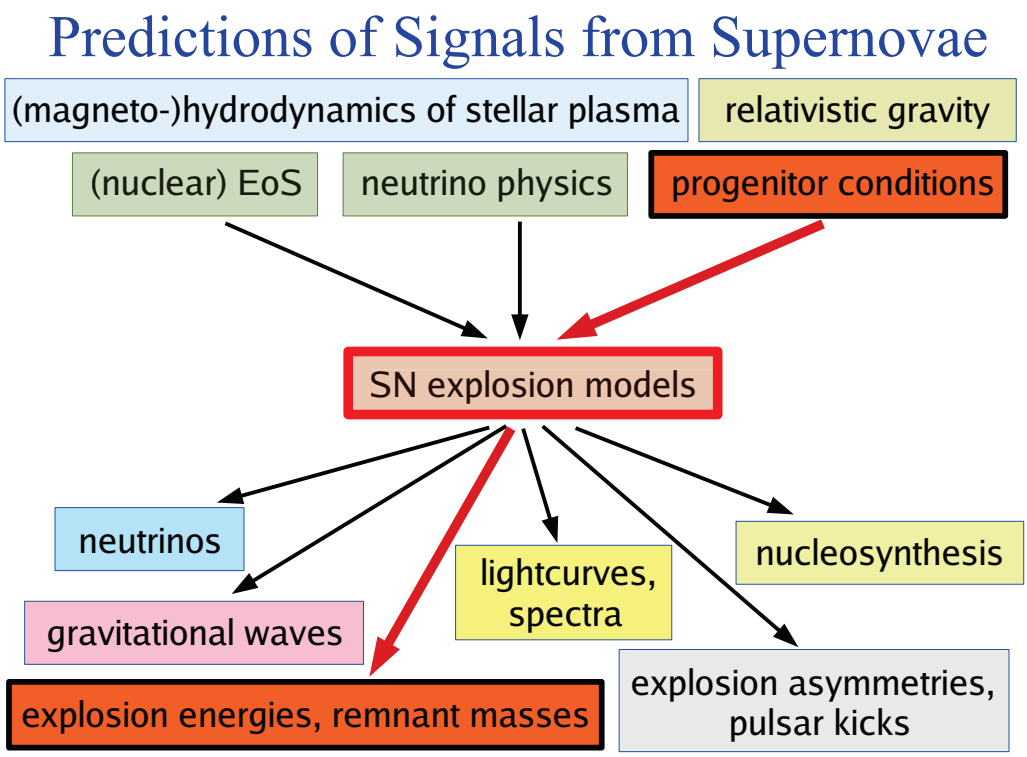

Fig. 4. Input and output from supernova explosion models. The predicted signals of stellar explosions depend on the complex interplay of a wide variety of input physics and require the knowledge of the initial conditions in the progenitor stars.

Sophisticated explosion models with all necessary theoretical ingredients are essential for a deeper understanding of observable phenomena and measurable signals associated with the death of massive stars and therefore also for developing a better definition of the role of supernovae in the astrophysical context (Fig. 4). One important aspect of the latter is the progenitor-explosion-remnant connection, which includes theoretical calculations of supernova energies, nucleosynthetic yields, and compact object masses in dependence of the properties of the progenitor stars. This problem is linked to the unsolved question which progenitors leave black holes behind instead of neutron stars. Self-consistent numerical simulations are especially needed when one aims for reliable predictions of neutrino signals and gravitational waves, which could be detected in the case of a future galactic event and would serve as valuable direct probes of the dynamical processes and thermodynamic conditions in the supernova core. As described above, also the conditions for the explosive creation of heavy elements are set by the interaction of the ejecta with the intense neutrino fluxes from the nascent neutron star. Moreover, the production of radioactive nuclei like ^{56}Ni as well as the nucleosynthetic reprocessing of the star's composition layers by the outgoing shock wave depend sensitively on the explosion energy and the location of the mass cut that separates the compact remnant from the supernova ejecta. Hydrodynamic instabilities during the first second of the explosion are responsible

for the observed large-scale explosion asymmetries that can lead to high pulsar recoil velocities.[29),31)–34)] By deforming the supernova shock they also seed the growth of secondary mixing instabilities at the composition shell interfaces after the passage of the explosion shock. These large-scale radial mixing processes destroy the onion-skin structure of the progenitor and carry heavy elements with high velocities from the region of their formation deep in the stellar core into the helium and hydrogen layers and, in turn, sweep hydrogen and helium inward in velocity as well as radial space. This compositional mixing and the large-scale explosion asymmetries have important consequences for the shape of supernova lightcurves, the characteristics of the supernova spectra, and the time evolution of the electromagnetic emission in different wave bands.

It is clear that final answers for the wealth of questions linked to all these issues will ultimately require a consistent as well as consolidated solution of the explosion mechanism of core-collapse supernovae. Admittedly, supernova theory is not yet there, but it has made good progress in directions that are promising for bringing us closer to the goal of our efforts. Despite the incompleteness of the present understanding of the problem at the heart of exploding stars, it still seems illuminative to explore possible implications and thus to move forward in assembling the pieces of a great puzzle, in which both theoretical and observational bricks need to be interweaved. While some adopt a pessimistic point of view and concentrate on the empty half of the glass, lamenting about a still imperfect match of modeling results with measured supernova properties and proclaiming solicitousness about what they, ostensibly, perceive as a defocussing and deception of the field by "myths that have crept into modern discourse",[35)] we prefer to look at current developments from a more optimistic perspective and to extract motivation from the fact that the glass seems to be half full at least. In this spirit a recent review article[2)] has highlighted advances that have happened over the past ten years. But also new challenges have emerged from the ambitious work of researchers around the globe, whose important contributions to various aspects of the field have refined our picture of stellar core collapse and the associated physical processes.

In the following brief, focussed overview, we shall summarize some of the latest results obtained by the Garching group and its collaborators. Although core-collapse theory is in rapid flow and the field is enthusiastically rushing towards more realism by advancing the models from two dimensions to three-dimensional space, basic physics that plays a role in the explosion mechanism does not depend on the considered dimension. Progress that has been achieved in the past, although necessarily obtained with constrained setups like axisymmetric (2D) simulations, will nevertheless provide the foundations for a better understanding of the crucial ingredients in a working supernova mechanism. In this sense we hope that the contents of this article will not grow stale too fast, despite the temporary nature of many modeling aspects and of conclusions that can be drawn still only from a narrowed perspective.

§2. Generic properties of the neutrino emission

It is now commonly accepted that the delayed neutrino heating mechanism is unable to yield explosions in spherical symmetry except for progenitors stars with O-Ne-Mg cores instead of Fe cores. These stars at the lower end of the mass range for supernova progenitors reach highly degenerate conditions already after central carbon burning so that electron captures on Mg, Na, and Ne begin to reduce the effective adiabatic index and enforce the collapse.[36] Since these progenitors possess an extremely steep density gradient around the core, the shock accelerates outward in response to the rapidly decaying mass accretion rate [cf. Eq. (1·1)] and neutrino energy deposition powers an outflow sufficiently strong to unbind the dilute He- and H-layers.[37] The energies of such explosions are, however, low (around 10^{50} erg, see Fig. 15 and Ref. 38)), and only little nickel is ejected (some $10^{-3}\,M_\odot$; Ref. 39)), for which reason the supernovae must be expected to be faint.

In all other progenitors multi-dimensional flows have turned out to be crucial for getting explosions. If large-scale nonsphericity, e.g. rotational deformation, is absent in the progenitor core, asymmetries must grow from small initial perturbations by hydrodynamic instabilities. During core infall, however, the conditions are not favorable for such a growth. The contracting flow remains essentially spherical (on large scales) up to core bounce. Moreover, during infall electron captures on heavy nuclei and free protons (the former dominate during most of the evolution) maintain a very similar structure of the homologously collapsing inner core, and the electron fraction converges to nearly the same central value ($Y_{e,\mathrm{c}} = 0.25$–0.27 for a central lepton fraction $Y_{\mathrm{lep,c}} = 0.28$–$0.30$; Ref. 43)) in different progenitors despite a small initial spread of values in the core center before collapse ($Y_{e,\mathrm{i}} \approx 0.425$–$0.445$) and considerable differences of the initial central entropy ($s \approx 0.6$–$1.2\,k_\mathrm{B}$ per nucleon). Since the mass of the homologous core scales with the instantaneous Chandrasekhar mass, $M_\mathrm{ic} \propto M_\mathrm{CH} \propto Y_e^2$, the baryonic mass enclosed by the shock formation radius is also very similar over a wide mass range of progenitor stars (from the same modeling set; Fig. 5). The shock formation position is defined here by the location where the postshock entropy first reaches $3\,k_\mathrm{B}$ per nucleon. The degree of

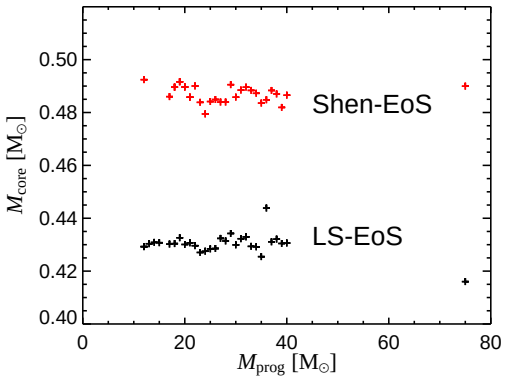

Fig. 5. Inner core masses enclosed by the shock-formation position in iron-core-collapse simulations of a large set of (solar metallicity) progenitor stars.[40] The point of shock formation (defined by the location where the postshock entropy first reaches $3\,k_\mathrm{B}$ per nucleon) depends on the deleptonization during collapse, which hardly varies with the mass of the progenitor. Also the EoS has an influence, connected to different collapse timescales and composition differences. We used the EoS of Ref. 41) in comparison to the EoS of Ref. 42) with compressibility modulus $K = 180\,\mathrm{MeV}$.

deleptonization during collapse, however, depends on the duration of the infall until neutrino trapping and on composition differences (especially the free proton fraction), both of which are connected to equation of state (EoS) properties (a detailed study can be found in Ref. 43)). Therefore the shock formation point is somewhat different for different EoSs ($\sim$0.43 $M_\odot$ vs. $\sim$0.49 $M_\odot$ in Fig. 5). In any case, however, the bounce shock is launched deep inside the stellar iron core, which makes it impossible for the shock to overcome the energy losses by nuclear photodisintegration processes in the massive, overlying shells of iron. With the small masses of the homologous inner core in current models, successful supernova explosions by the hydrodynamical bounce-shock mechanism are ruled out.

After a short phase of maximum strength, the bounce shock is weakened again by the drain of nuclear energy. A negative entropy gradient emerges in the shock deceleration region, which quickly decays in a short (typically 30–50 ms) phase of "prompt postshock convection". This phase makes a gravitational wave signal[44] but has only a weak influence on the neutrino emission. Somewhat later, neutrino heating behind the shock grows in strength because the postshock temperature drops and the mean energies of the radiated neutrinos continuously rise with time (Figs. 6 and 7). A gain layer forms and a local entropy maximum builds up just outside the gain radius and creates the necessary (and in most cases sufficient) condition for the onset of convective overturn in the accretion layer behind the stalled shock. First Rayleigh-Taylor fingers show up typically 80–100 ms after bounce, but it can take roughly another $\sim$100 ms before the accretion flow in the postshock layer becomes largely perturbed by convective downdrafts and buoyant plumes. On a similar timescale also the SASI grows and can manifest itself (at least in two dimensional (2D, i.e., axisymmetric) models) by pronounced sloshing motions of the shock surface (for a detailed numerical study of neutrino-driven convection and the SASI and their interaction in 2D core-collapse simulations, see Refs. 17), 26)). Besides the convective overturn in the neutrino-heating layer, convection also develops in the deleptonization region inside the neutrinospheres.[13),45)] Associated effects on the neutrino emission, for example an increase of the heavy-lepton neutrino fluxes and a reduction of the $\bar{\nu}_e$ flux compared to the nonconvective proto-neutron star, however, are also small in the first $\sim$100 ms after core bounce.[13)]

During this early postbounce period of up to about 100 ms, spherically symmetric models therefore yield reliable information about the neutrino emission properties. We display corresponding information on the radiated luminosities and mean spectral energies (for an observer at rest at a large distance from the source) for all neutrino species in Figs. 6 and 7. (Muon and tau neutrinos and antineutrinos have very similar opacities and are lumped together to one kind of heavy-lepton neutrino, ν_x.) In the first case the relatively stiff nuclear (EoS) of Ref. 41) was used, in the second case the considerably softer one*) of Ref. 42). These images should be compared

*) Somewhat unconventionally, we use the terms "stiff" and "soft" for the EoS to classify the *radius evolution* of the forming neutron star with the corresponding EoS, "soft" meaning that the nascent remnant *contracts faster* to its final radius. Note that a "soft" EoS in our sense *neither* means that the maximum neutron star mass is low *nor* that the final neutron star radius is particularly small. Physically, the maximum mass of the neutron star is determined by the supernuclear

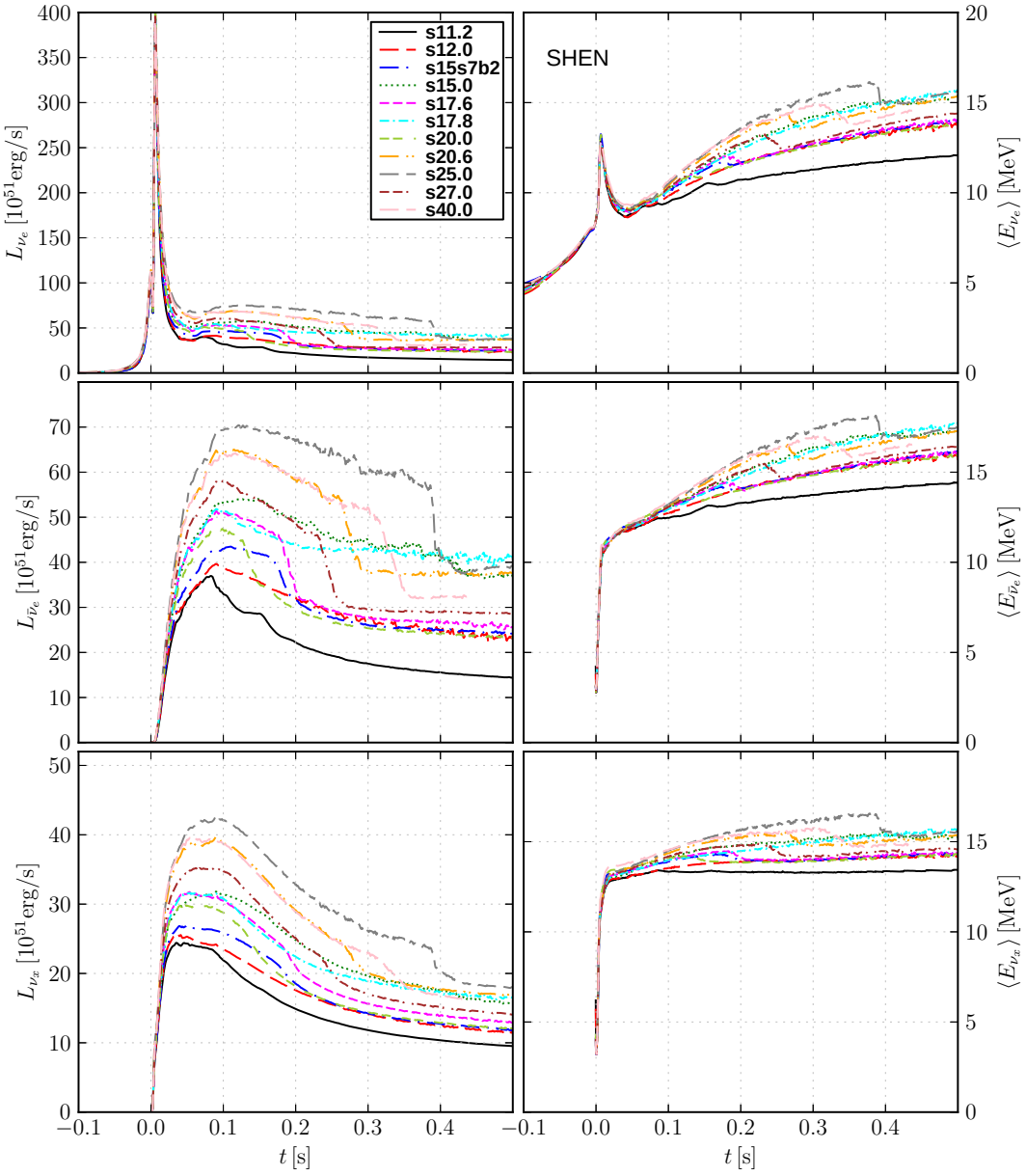

Fig. 6. Time evolution of luminosities (*left*) and mean energies (defined as ratio of energy flux to number flux; *right*) for ν_e (*top*), $\bar{\nu}_e$ (*middle*), and one kind of heavy-lepton neutrino (all treated equally; *bottom*) as measured in the lab frame at infinity. Time is normalized to the moment of core bounce. The results are plotted for (nonexploding) 1D simulations of a set of solar-metallicity progenitors[40] and an older 15 $M_\odot$ progenitor (s15s7b2; Ref. 46)), applying the EoS of Ref. 41).

properties of cold neutron star matter, whereas the radius evolution of the nascent compact object strongly depends on how the conditions in matter at subnuclear densities depend on changes of the temperature and of the neutron-to-proton ratio (both are evolving in response to neutrino emission).

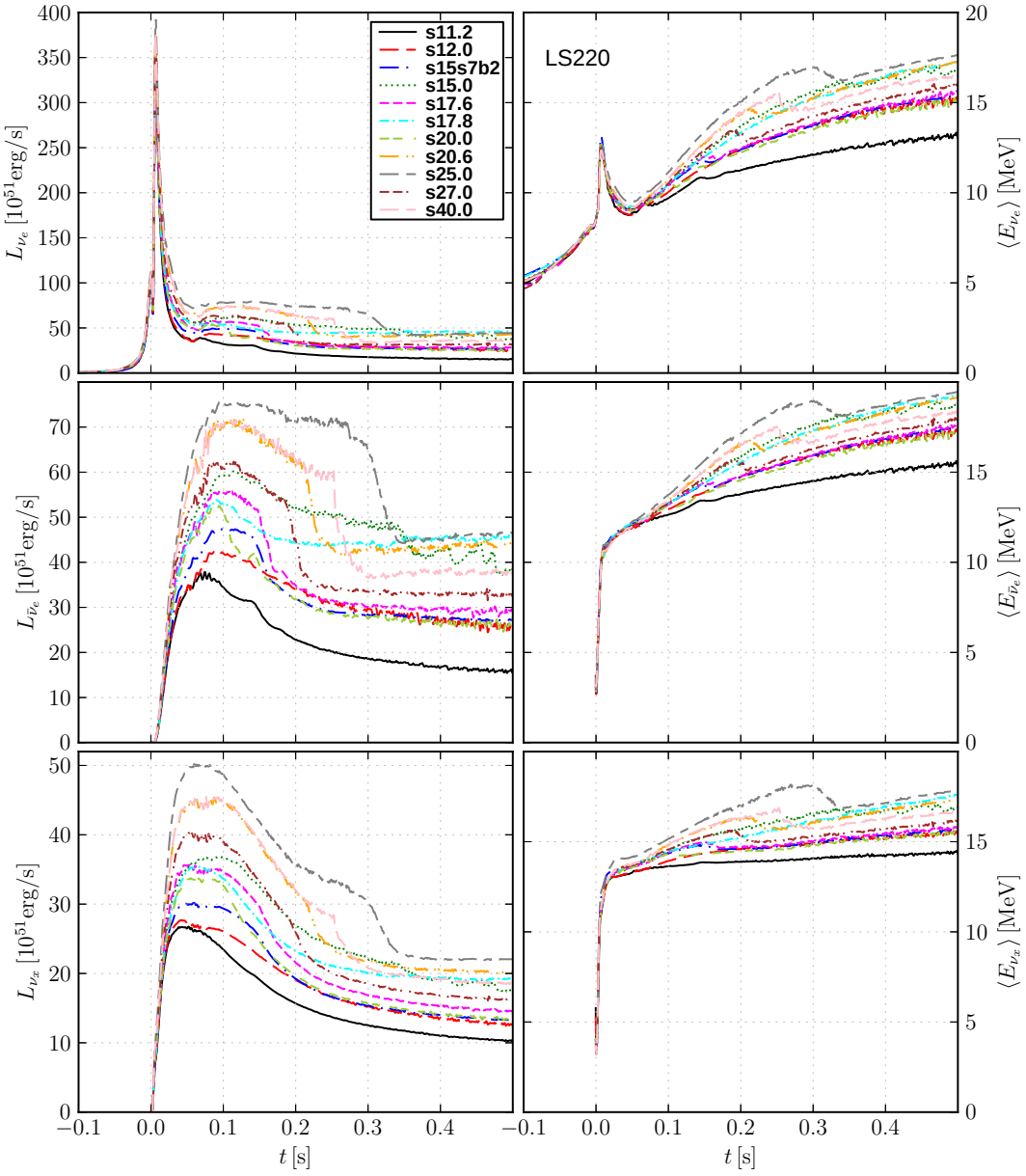

Fig. 7. Same as Fig. 6, but for (nonexploding) 1D simulations with the EoS of Ref. 42) using a compressibility modulus of $K = 220$ MeV. This EoS is softer than the one used in Fig. 6.

with Fig. 3 in Ref. 47). Although our set of core-collapse calculations and the one of Ref. 47) employ different series of progenitor models, basic features of the neutrino signal are generic and, even more, general trends should be comparable even beyond 100 ms after bounce, despite the disregard of multi-dimensional effects.

It should be noted that our calculations were performed with the PROMETHEUS-VERTEX code with general relativistic corrections,[4] which performed very well in tests against fully relativistic treatments.[6),48),49)] The energy-dependent three-flavor

neutrino transport module is based on a two-moment closure scheme with a variable Eddington factor derived from a model-Boltzmann equation. The transport includes velocity-dependent terms, energy-bin coupling, and the full set of neutrino opacities[5] (see Fig. 3).

Although in Ref. 47) a variety of simplifications were applied (e.g., a subset of neutrino processes was used and velocity-dependent effects were ignored in the transport), the overall evolution of the neutrino emission properties of ν_e and $\bar{\nu}_e$ is reproduced relatively well. This outcome is connected to the facts that on the one hand electron-flavor neutrinos mainly interact by the charged-current absorption and emission processes and on the other hand the neutrinos escape from regions near the proto-neutron star surface, where the matter is essentially at rest. Features that depend on the motion of the stellar medium, however, are absent in the results of Ref. 47). One example is the characteristic local minimum of the ν_e luminosity shortly after core bounce and before the luminosity rises steeply to its prominent maximum. In this feature the luminosity drops from $\sim 1.15 \times 10^{53}\,\mathrm{erg\,s^{-3}}$ to $\sim 0.7 \times 10^{53}\,\mathrm{erg\,s^{-3}}$ (which can easily be seen only on a zoom to its location). This dip is formed about 1 ms after bounce and approximately another millisecond before shock breakout from the neutrinosphere (where the optical depth decreases to about unity). At this time the shock is still deep in the optically thick region and the neutrinos produced behind the shock are still trapped. Most of the ν_e release therefore comes from the compressed, unshocked and semitransparent layer around 100 km. When the matter in this layer falls inward with increasingly higher speed, the emission gets more and more redshifted due to the Doppler effect and, moreover, an increasing fraction of the neutrinos is advected inward with the gas flow. These effects lead to the transient luminosity reduction before the rise to the shock-breakout burst sets in.

The ν_e signal through core collapse, bounce, and shock breakout is extremely similar for all progenitors and also for different EoSs.[50] Even during the first $\sim$100 ms after bounce the progenitor stars have little influence on the mean energies of the radiated neutrinos of all kinds, although the luminosities already begin to exhibit a spread that reflects the different mass infall rates in the cores of different stars. More compact progenitor cores[*] lead to higher mass accretion rates of the nascent neutron star, which in turn produces higher neutrino luminosities supplied by the emission of neutrinos from the hot, lepton-rich, freshly accreted material. Higher stellar core compactness systematically correlates with higher luminosities of all neutrino species.[47]

At times $t \gtrsim 100$ ms post bounce, consequences of multi-dimensional effects on the neutrino emission cannot be ignored any longer.[13),15),52] The radiated neutrino signal is then affected by convection inside the neutron star, which raises the heavy-lepton neutrino fluxes, reduces the $\bar{\nu}_e$ emission, and decreases the mean energies of the escaping neutrinos.[13),52] The neutrino emission is also modified and mod-

[*] Compactness is measured by the ratio of mass to corresponding radius enclosing this mass. Higher compactness means that more mass falls inward in a certain time. For a definition and discussion of the compactness in the context of black hole formation, see Ref. 51).

ulated by nonspherical accretion downflows, which are associated with anisotropic, transient, short "bursts" of accretion luminosity.[52)–55)] Nevertheless, some general properties can be discussed that are shared by 1D as well as angle-averaged 2D and 3D results.

At $t \gtrsim 100\,\mathrm{ms}$ post bounce also the mean energies of the radiated neutrinos begin to exhibit a spread that reflects the core compactness. Higher core compactness and higher mass accretion rates do not only produce higher neutrino luminosities but also larger mean energies of the emitted neutrinos. While before $t \sim 100\,\mathrm{ms}$ p.b. the nascent neutron stars in all progenitors are still relatively similar, the different mass accretion rates in stars with different core compactnesses cause the proto-neutron star masses to become increasingly different. For this reason the mean energies develop a growing spread with time: More massive proto-neutron stars possess hotter neutrinospheres and the mean neutrino energies increase more steeply than in the case of less massive neutron stars in less compact progenitors. The collapsing cores of such less compact stars feed the growth of the neutron star mass with rapidly decreasing rates at late postbounce times. Interestingly, in all cases (and for both stiff and soft neutron star EoS) there is a point during the late accretion phase when the mean energy of $\bar{\nu}_e$ crosses and subsequently exceeds the mean energy of the heavy-lepton neutrinos. The physical reason for this effect was discussed in Ref. 52). After the explosion has taken off and the accretion has ended, the mean energies adopt again the well known hierarchy, where $\langle\epsilon_{\nu_e}\rangle < \langle\epsilon_{\bar{\nu}_e}\rangle < \langle\epsilon_{\nu_x}\rangle$.

It should be noticed that in Ref. 47) —presumably because of the approximations in the neutrino transport used there— considerably higher mean neutrino energies are predicted for the later postbounce evolution (compare Fig. 3 in Ref. 47) with Figs. 6 and 7 in our paper*)). In particular, also the differences between the core-collapse models with soft and stiffer EoS tended to be larger in Ref. 47). The authors of the latter paper proposed to use the cumulative neutrino energy from the postbounce accretion phase, which correlates with the mass accretion rate of the progenitor, to obtain information of the core structure of the collapsing star in the case of a neutrino measurement from a future galactic supernova. In order to break the degeneracy between nuclear EoS and progenitor-core compactness (a higher neutrino luminosity and number flux, for example, can be caused by a larger mass accretion rate or by a softer EoS), they suggested to combine the measurement of the cumulative energy (or cumulative event number) with the information about the mean energy of the neutrinos. In view of the weak sensitivity of the mean energy to the EoS (cf. Figs. 6 and 7) such a discrimination will be quite an ambitious undertaking.

*) Note that the comparison between the different transport solvers in Fig. 2 of Ref. 47) was done with a reduced set of neutrino opacities instead of the more sophisticated and larger set of neutrino reactions usually applied in the simulations of the Garching group. Moreover, the approximate description of general relativistic gravity used in the PROMETHEUS-VERTEX calculations of Ref. 48) (referred to in Ref. 47)) was subsequently improved by Marek et al.,[49)] whose preferred description was shown to lead to much better agreement with fully relativistic results.[6)]

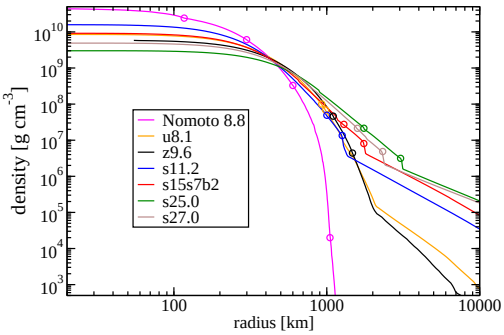

Fig. 8. Pre-collapse density profiles of progenitor stars used for the 2D explosion models of Figs. 10–15. The circles mark the boundaries of the Fe-core and the Si/Si+O interface in the solar-metallicity 11.2 $M_\odot$ (s11.2), 25 $M_\odot$ (s25.0), and 27 $M_\odot$ (s27.0) models,[40] in the 15 $M_\odot$ (s15s7b2) model,[46] and in the ultra-metal poor (10^{-4} solar) 8.1 $M_\odot$ progenitor,[56] whereas they indicate the Fe/Si and Si/O+N transitions in the zero-metallicity 9.6 $M_\odot$ (z9.6) star.[56] In the 8.8 $M_\odot$ progenitor with O-Ne-Mg core[36] the circles denote the composition changes from NSE to Ne+O, then to Ne+Mg+O, to C+O, and finally to He.

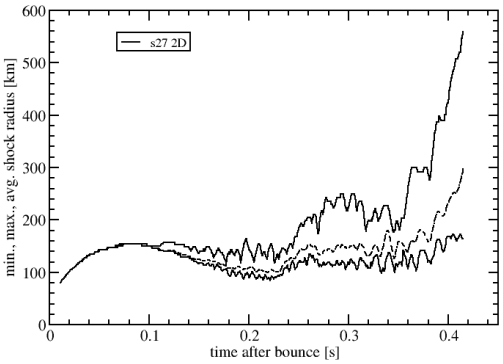

Fig. 9. Postbounce evolution of the maximum, minimum and average shock radius in a 2D simulation of the 27 $M_\odot$ progenitor of Fig. 8 with the Prometheus-Vertex code, which employs an approximate treatment of general relativistic effects in the gravitational potential and neutrino transport. As in the fully relativistic 2D simulation shown in Fig. 10, bottom right panel, a neutrino-driven explosion takes place, although the runaway shock expansion sets in somewhat later and after less vigorous bipolar shock oscillations than in the relativistic calculation.

§3. Relativistic explosion models in two dimensions

Successful neutrino-driven explosions cannot be obtained in 1D with the neutrino heating associated with the neutrino emission properties of present models as discussed in Sect. 2. The Garching group, however, has recently found explosions for a growing set of progenitor stars with different masses (8.1, 8.8, 9.6, 11.2, 15, and 27 $M_\odot$) and metallicities (Fig. 8) in 2D simulations with the general relativistic CoCoNuT-Vertex hydrodynamics and neutrino transport code.[6),16),17),44)] These results can be considered as a basic confirmation of the self-consistent 2D explosion models of 11.2 $M_\odot$ and 15 $M_\odot$ stars computed with the Prometheus-Vertex code by Buras et al.[13)] and Marek & Janka.[15)] Also the 27 $M_\odot$ explosion has recently also been reproduced (Fig. 9) with the Prometheus-Vertex tool, which employs a relativistic approximation of the gravity potential[49)] and relativistic corrections in the transport module.[4)] Despite differences in details, e.g. in the postbounce dynamics and explosion times of 2D models with general relativistic and approximate relativistic treatment, there seems to be overall agreement and compatibility of the results obtained with these two different numerical schemes*).

*) The Prometheus-Vertex and CoCoNuT-Vertex codes do not only differ in the treatment of general relativity, they also employ largely different hydrodynamics solvers, cf. Refs. 4) and 6).

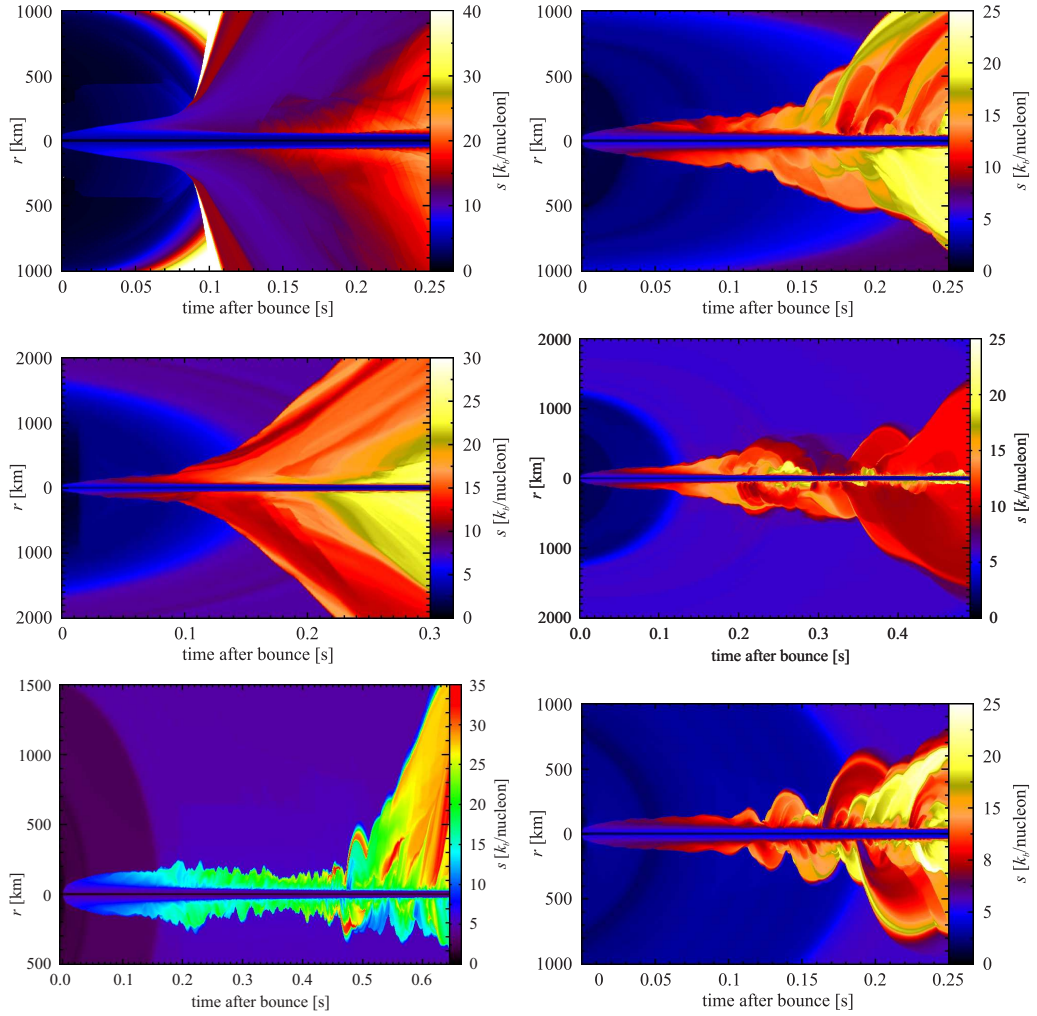

Fig. 10. Time evolution after core bounce of the profiles of entropy per nucleon in north-polar and south-polar directions for 2D (general relativistic) explosion simulations[16),17),44)] of the 8.8 $M_\odot$ ONeMg-core progenitor and the 8.1 $M_\odot$, 9.6 $M_\odot$, 11.2 $M_\odot$, 15 $M_\odot$ and 27 $M_\odot$ Fe-core stars with different metallicities (*from top left to bottom right*) shown in Fig. 8. Dark blue and black represent low-entropy unshocked matter while green, yellow, and red indicate hot, high-entropy matter. Bipolar shock oscillations suggest SASI activity.

Entropy profiles in the north and south polar directions as functions of post-bounce time are displayed for the relativistic explosion models in Fig. 10. Corresponding Y_e and entropy distributions for representative instants near the end of the simulated postbounce periods are given in Fig. 11[*)]. Of the set of progenitors investigated so far, only the 25 $M_\odot$ did not show any tendency of an explosion and looks very disfavorable for a final success when the computational run was stopped at 450 ms after bounce (Fig. 12). This can be seen in Fig. 14, which shows a very

[*)] Note that the explosion simulation for the 8.8 $M_\odot$ progenitor with O-Ne-Mg core was performed with the relativistic approximations of the PROMETHEUS-VERTEX scheme.

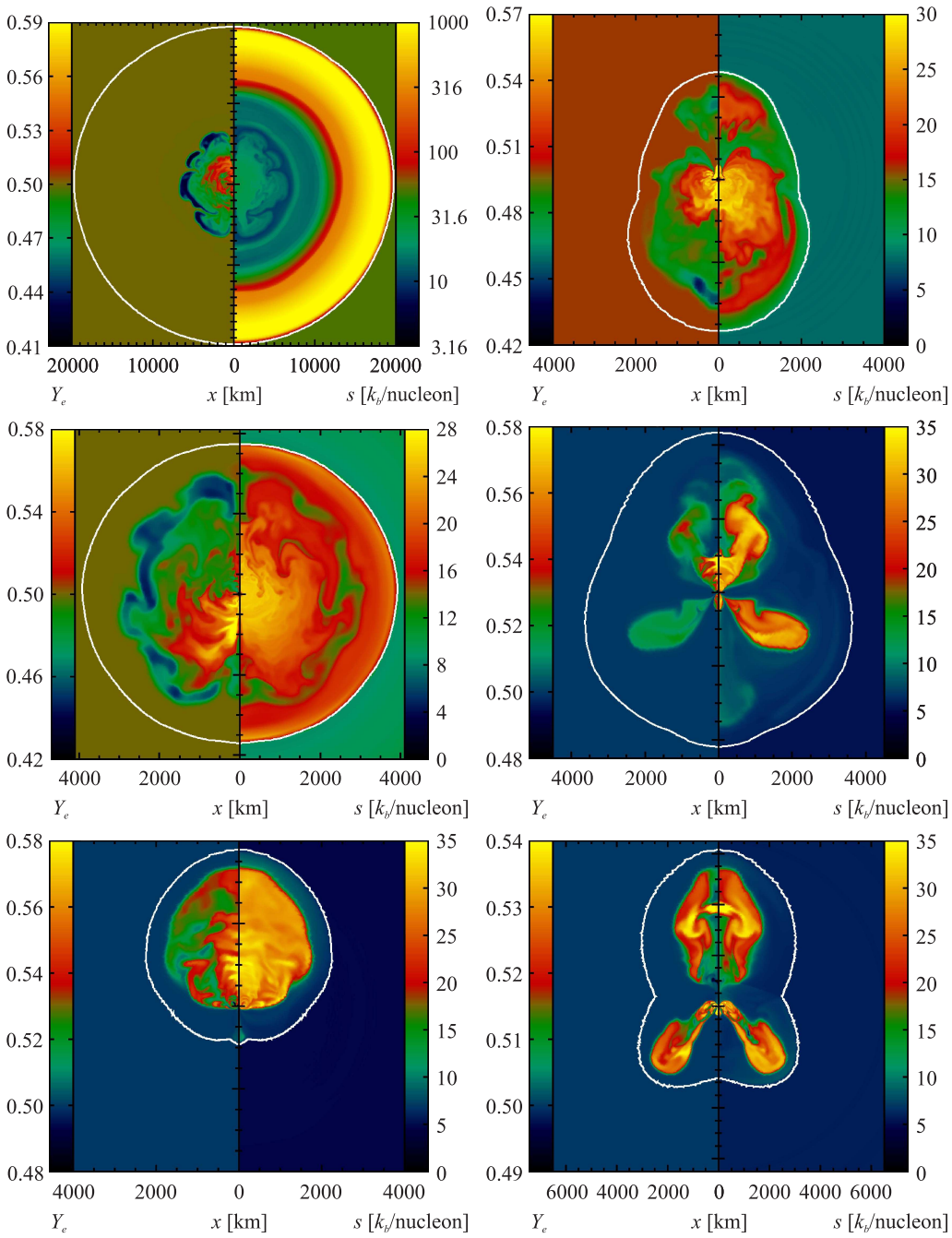

Fig. 11. Cross-sectional distributions of electron fraction (left half panels) and entropy per nucleon (right half panels) for the simulations shown in Fig. 10 (*from top left to bottom right* for 8.8, 8.1, 9.6, 11.2, 15, and 27 $M_\odot$ progenitors) at postbounce times near the end of the simulations: $t_{\rm pb} = 365$ ms, 330 ms, 318 ms, 920 ms, 775 ms, and 790 ms, respectively. The supernova shock is marked by a thin white line. High-entropy bubbles of neutrino-heated, expanding matter drive aspherical shock expansion in most cases.

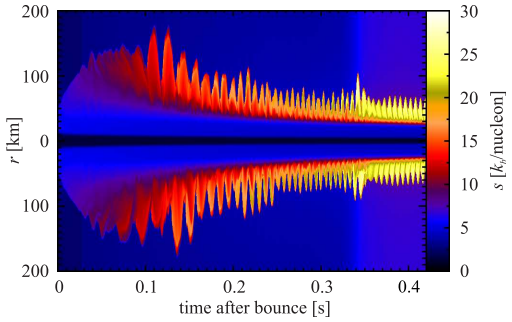

Fig. 12. Same as Fig. 10, but for the non-exploding solar-metallicity $25\,M_\odot$ star of Fig. 8. Alternating north-polar and south-polar shock excursions indicate violent SASI sloshing motions.

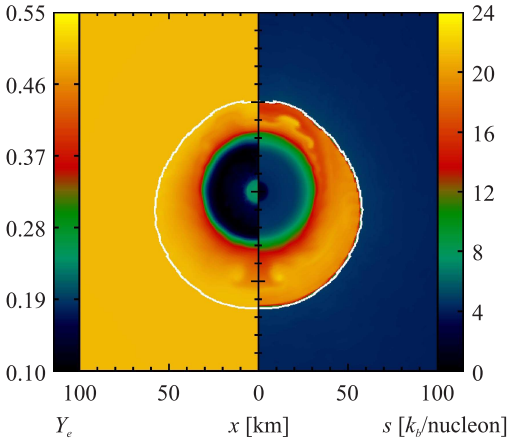

Fig. 13. Same as Fig. 11, but for the nonexploding solar-metallicity $25\,M_\odot$ model of Fig. 12 at 309 ms post bounce. The postshock layer is very narrow and the rapid infall velocities of the fluid between shock and gain radius suppress the growth of neutrino-driven convection. The entropy structures in the postshock layer are mainly linked to Kelvin-Helmholtz instability associated with strong shear effects at the interface of differentially moving regions in the sloshing flow.

small maximum radius of the shock in the $25\,M_\odot$ case, while in all other relativistic 2D models the shock expands with high velocities of at least 6000–7000 km s^{-1}, in most cases much faster. The explosions develop on different timescales, depending on the different density profiles and locations of the composition shell interfaces, which determine the decay of the expansion-damping mass accretion rate. (Remember that according to Eq. (1·7) the critical luminosity is larger for higher $\dot{M}$ and bigger neutron star mass, which also grows faster for high $\dot{M}$.) The decrease of the mass accretion rate with time competes with the progenitor-dependent evolution of the neutrino emission properties (cf. Figs. 6 and 7), which decide about the strength of the neutrino energy deposition. If the critical condition for an explosion in 2D is met at some point, the model makes the transition to a runaway expansion of the supernova shock. In the $25\,M_\odot$ star with its highest compactness (Fig. 8) the large mass infall rate (and quickly growing neutron star mass) prevent an explosion until the end of our computation.

In Fig. 15 the "diagnostic energies" are given for the successful cases. The diagnostic energy at each time is defined as the total energy (internal plus gravitational plus kinetic) of all postshock material with positive radial velocity and and positive total specific energy. This is not yet the explosion energy of the supernova, because the positive energies may still increase by ongoing neutrino heating of accreted and then reejected gas, by additional energy associated with the neutrino-driven wind

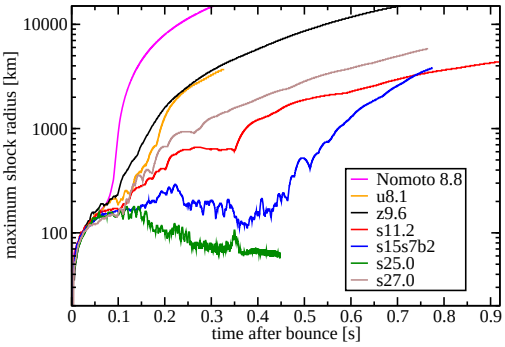

Fig. 14. Maximum shock radii versus time for the set of 2D explosion models of Figs. 10 and 11 and for the nonexploding 2D model of Figs. 12 and 13.

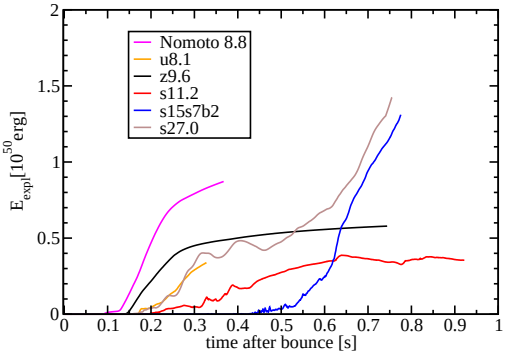

Fig. 15. Evolution of the "diagnostic" explosion energy (i.e., the energy of outward expanding postshock matter with positive specific energy) versus time for the set of models of Fig. 14.

material, by the recombination of free nucleons and α particles to heavy nuclei, and by nuclear burning in the shock-heated layers (see Sect. 1). Moreover the binding energy of the outer stellar layers (still ahead of the shock) will contribute on the negative side and has to be overcome to make the star unbound for an explosion with excess kinetic energy at infinity. While this binding energy is negligible for the $8.8\,M_\odot$ progenitor (whose O-Ne-Mg core is surrounded by an extremely dilute and loosely bound H-shell) and small for the lower-mass iron-core stars (i.e., less than $\sim 3 \times 10^{48}$ erg in the $8.1\,M_\odot$ case and even less for the $9.6\,M_\odot$ star), the binding energy of the stellar mantle and envelope can be appreciable for more massive progenitors. In the $11.2\,M_\odot$ and $15\,M_\odot$ models, for example, the binding energies of the preshock shells are 7.5×10^{49} erg and 2.6×10^{50} erg, respectively, whereas the still available recombination energies of the postshock matter are 2×10^{49} erg and 1–2×10^{50} erg.[16] In the case of the $15\,M_\odot$ and $27\,M_\odot$ models the diagnostic energies are still steeply increasing at the end of the simulations and the terminal values cannot be guessed. In contrast, the diagnostic energies of the other models begin to saturate. The explosions will therefore become relatively weak, and a lot of fallback has to be expected.

§4. Magnetically supported explosions in nonrotating progenitors

Magnetic fields are known to be strongly amplified during the secular postbounce evolution of rapidly differentially rotating, collapsing stellar cores. Besides compression upon infall, the amplification is mainly achieved by field winding in shear layers and the magnetorotational instability (MRI), see e.g., Refs. 57), 58). One may ask, however, how strong the fields have to be, and how strong the corresponding initial fields, if magnetic effects are to have an impact on the development of the explosion in nonrotating (or very slowly rotating) stellar cores. Slow core rotation is predicted by evolution models of magnetized, massive stars[59] because of angular momentum

loss mainly during the red-giant phase. With predicted pre-collapse spin periods of more than hundred seconds in the iron core, the postshock layer attains rotation periods of hundreds of milliseconds to many seconds and possesses only tiny amounts of free energy of rotation (which is the reservoir to be tapped for field amplification). In this case neither wrapping nor the MRI are efficient mechanisms to enhance the field strength.

Obergaulinger & Janka[60] have recently investigated the effects of magnetic fields on the shock evolution in nonrotating stellar cores*). In this case the amplification of the fields in the gas flow relies on two processes:

- Compression of the fields against the magnetic pressure increases the magnetic energy density $e_{\rm mag}$; magnetic energy is created by this process at a rate $s_{\rm cmp} = -e_{\rm mag}\vec{\nabla}\cdot\vec{v}$.
- Stretching and folding of the field lines, in which case the energy density of the field can be amplified at a rate of $s_{\rm str} = B^i B^j \nabla_j v_i$. This process is the main ingredient of a turbulent dynamo.

The amplification by compression takes place in the converging flow of the unshocked, infalling layers, in the flow passing the shock, and in convective downdrafts in the postshock region. Turbulent mass motions due to neutrino-driven convection and the SASI[61),62)] lead to further amplification by dynamo action in the region between stalled shock and protoneutron star.

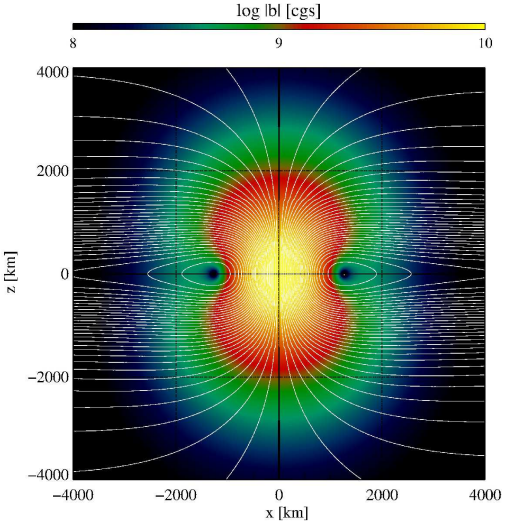

Fig. 16. Field lines and field strength (color-coded) with central value of $B_{\rm c} = 10^{10}$ G assumed for the initial (pre-collapse) field configuration of a $15\,M_\odot$ progenitor.[40)] Initial configurations with other central field values used in our simulations are obtained by simple scaling. In our nonrotating stellar cores we have adopted a purely poloidal field. This is clearly artificial and besides the experimental purpose the assumed absence of stellar rotation to create toroidal field components might serve as justification. A high-resolution version of this figure is available upon request.

Figure 17 shows the postbounce evolution of four simulations of a $15\,M_\odot$ progenitor, comparing the nonmagnetic case with three cases for different initial magnetic field strengths, corresponding to central field values of 10^{11} G, $10^{11.5}$ G, and 10^{12} G. The assumed pre-collapse field configuration in the stellar core is displayed in Fig. 16. The panels of Fig. 17 visualize the time dependence of the radial profiles of angularly averaged entropy and magnetic field values (or Y_e in the nonmagnetic case). Spatial distributions for representative

*) The results discussed here are based on simulations with higher resolution and a two-dimensional, multi-energy-group, two-moment closure scheme for neutrino transport, which was upgraded relative to the models in Ref. 60). The improvements will be entered in a revised version of the latter paper.

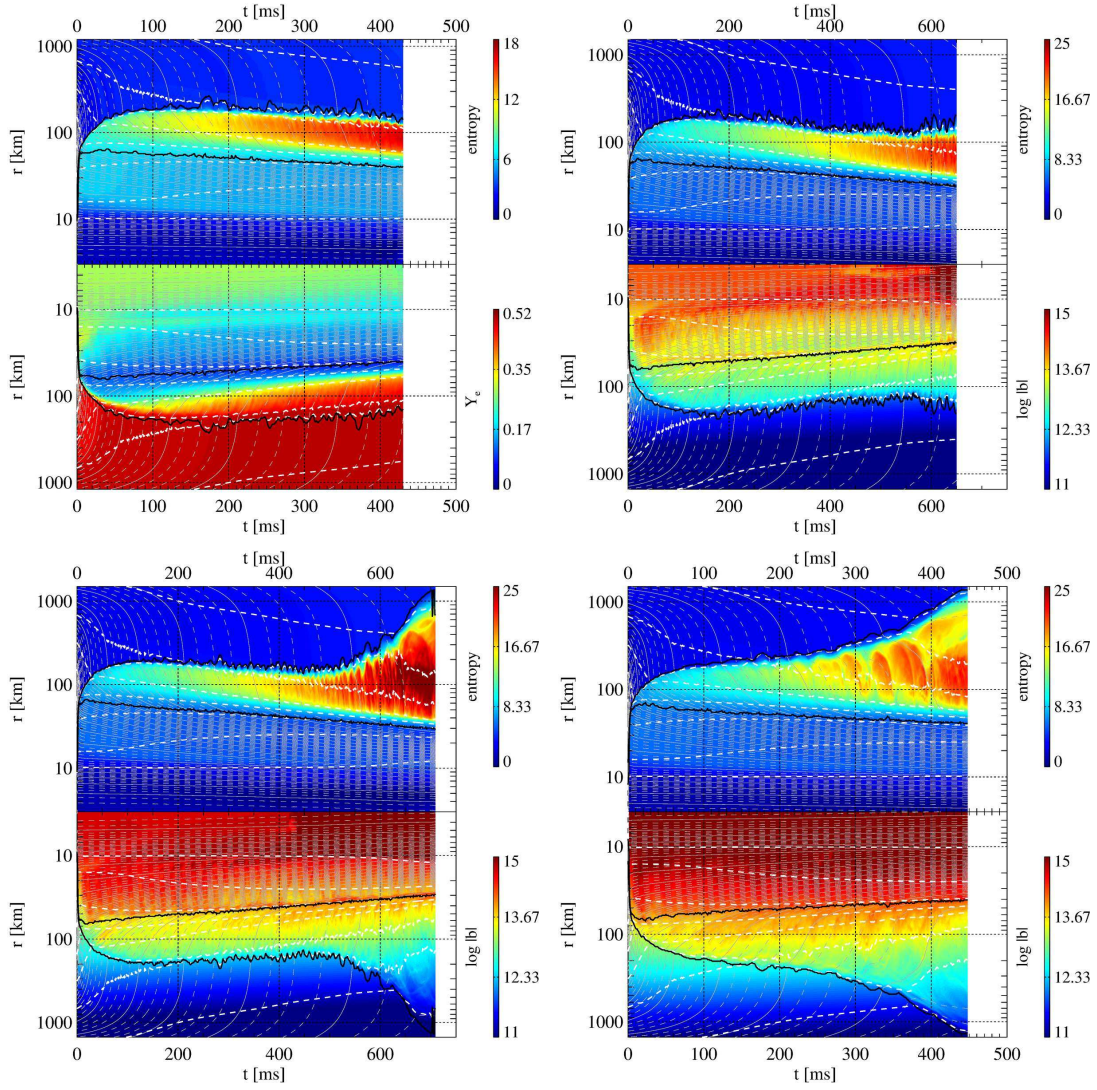

Fig. 17. Postbounce evolution of 2D simulations for a $15\,M_\odot$ progenitor[40] with different assumptions of the initial magnetic field strength for central values of $B_c = 0$ (*top left*), 10^{11} G (*top right*), $10^{11.5}$ G (*bottom left*), and 10^{12} G (*bottom right*). In the case of the nonmagnetized model, radial profiles of the angular averages of entropy per baryon (upper half panel) and electron fraction, Y_e, are color-coded, whereas for the magnetized models Y_e is replaced by the logarithm of the angularly averaged magnetic field strength. Note that the ordinate with the radius has been mirror imaged in the lower half-panels. The thin grey lines indicate trajectories for different fixed values of the enclosed mass spaced in steps of $0.025\,M_\odot$ (dashed) and $0.1\,M_\odot$ (solid). The two black lines denote the maximum radius of the shock front and the outer edge of the convection zone inside of the proto-neutron star, respectively. The white dashed lines mark locations of chosen constant values of the angle-averaged mass density for $\rho = 10^{14}$, 10^{13}, $10^{12}\,\mathrm{g\,cm^{-3}}$, etc. from the center outwards. The amplification of the initial core field during collapse, shock compression, and turbulent folding fosters shock expansion and the initiation of neutrino-powered explosions on a timescale that decreases with the strength of the magnetic field (compare left lower and right lower panels).

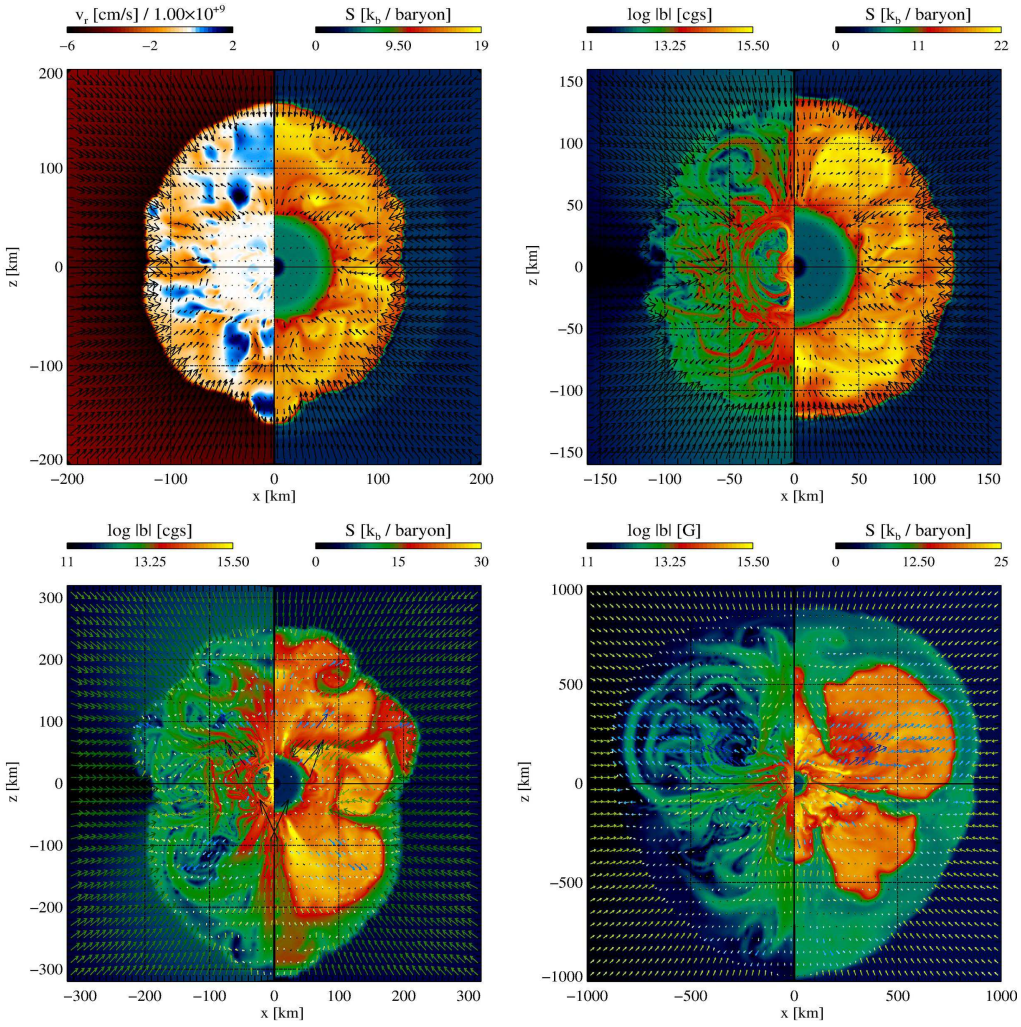

Fig. 18. Representative snapshots for the simulations displayed in Fig. 17. For the nonmagnetized model the radial velocity (left half panel) and the entropy per nucleon (right half panel) are shown; for the models with magnetic fields the logarithm of the magnetic field strength is color-coded instead of the radial velocity. Arrows indicate the flow field. The chosen postbounce times are 400 ms, 512 ms, 574 ms, and 412 ms (from top left to bottom right), respectively. Neutrino-heated, high-entropy gas rises in buoyant bubbles and pushes the shock expansion. The magnetic field structure in the postshock layer traces the convective pattern of bubbles and downflows and tends to be stronger in the compression regions of the downdrafts.

times are presented in Fig. 18.

In the lower two panels of Fig. 17 the shock evolution is clearly affected by the presence of the magnetic fields. The shock radius is larger compared to the nonmagnetic model (upper left panel) and ultimately the shock begins to expand, followed by the gas in the postshock region. While for an initial central field strength of 10^{12} G the shock expansion becomes strong about 200 ms after bounce (bottom right), a powerful shock expansion sets in only 500 ms after bounce for initial central

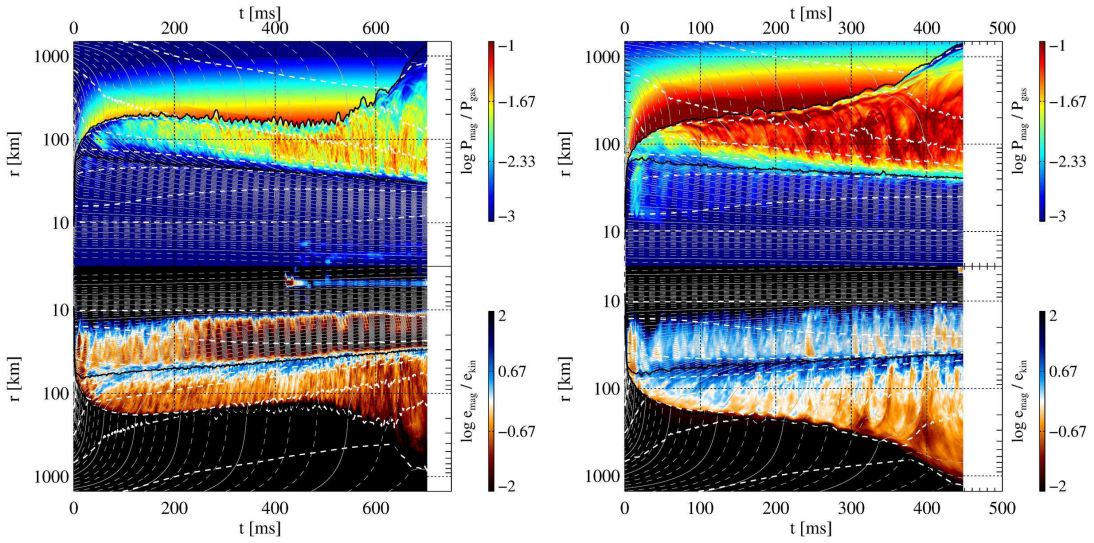

Fig. 19. Postbounce evolution of the 2D simulations with initial central magnetic fields of $10^{11.5}$ G (*left*) and 10^{12} G (*right*). The upper half-panels show the color-coded logarithm of the ratio of magnetic pressure to gas pressure, the lower half-panels display the logarithm of the ratio of magnetic energy density to kinetic energy density. The shock expansion is supported by significant magnetic pressure (between several per cent and ∼10% of the gas pressure) in the postshock layer. The field there reaches equipartition strength with the kinetic energy of the flow.

field strength of $10^{11.5}$ G (bottom left). For even weaker initial field ($B_c = 10^{11}$ G; upper right panel) one can see first hints for a transition to shock expansion after nearly 600 ms. The onset of shock acceleration is associated with the development of positive total energy in the expanding postshock material. This growth of the energy signals the beginning of an explosive runaway.

The dynamical relevance of the magnetic field can be expressed by the ratio of magnetic field pressure to the gas pressure, whose radial profiles are plotted as function of time for the two exploding models with highest fields in the upper half-panels of Fig. 19. Postshock fields of about 10^{13} G (Fig. 17) correspond to a magnetic pressure contribution to the gas pressure of several per cent up to about 10%. This obviously is sufficient to play a dynamically important role and to support the shock expansion. As a consequence, the inflation of large bubbles of neutrino-heated, high-entropy gas is enabled and the flow in the accretion region between shock and gain radius becomes much more ordered, with a dominance of low-order spherical harmonics modes in the convective pattern (Fig. 18). As the shock propagates outward, the push of the rising bubbles of heated matter becomes the driving force for further expansion, because the relative importance of the magnetic pressure to the gas pressure behind the outward rushing shock quickly decreases. The lower half-panels of Fig. 19 demonstrate that in the turbulent postshock layer prior to the onset of the explosion the average magnetic field grows to a value near equipartition with the amplification-supporting average density of kinetic energy.

Despite the constraint of our models to 2D and the unavoidable limitations of

the resolution, we think that one can conclude that the magnetic field amplification in collapsing stellar cores, even in the absence of any significant amount of initial core rotation, can lead to dynamical effects on the evolution of the supernova shock. For sufficiently strong initial fields magnetic pressure in the postshock layer can support the onset of neutrino-powered explosions on relevant timescales (of order 0.5–1 s after core bounce). Further simulations, in particular also 3D models with more realistic initial conditions for the field strength and geometry based on stellar evolution predictions,[59] are needed to clarify whether this could play a relevant role as ingredient in the neutrino-driven explosion mechanism.

§5. Convection or SASI as trigger of shock expansion?

A detailed discussion and analysis of the postbounce dynamics leading to the onset of explosions in the 2D models of Sect. 3 (including a description of the associated gravitational-wave signals) is provided in Refs. 15)–17), 44). Some of the plots of the entropy evolution in Figs. 10 and 12 as well as corresponding movies show violent bipolar sloshing motions of the shock and of the matter in the postshock layer.

These bipolar shock oscillations are found to exhibit growing amplitudes before neutrino-powered explosions set in. Such a behavior is visible in the $11.2\,M_\odot$ and $15\,M_\odot$ cases,[15),16)] but the alternating up and down motions of the shock are especially prominent in the $27\,M_\odot$ model,[17)] where the extremely high infall velocities in the postshock flow suppress the growth of neutrino-driven convection in the first place, unless large initial entropy perturbations drive non-linear buoyancy from the beginning (for a discussion of the necessary conditions, see Refs. 13), 17), 26), 63)). In this case the SASI-typical oscillatory increase of the amplitude of low-order shock deformation modes appears very clearly. In contrast, the dynamics of the lower-mass progenitors does not exhibit this characteristic behavior or, at least, it is not present there in such a pure form (Fig. 10). Buras et al.[13)] found shock oscillations with large dipole ($\ell = 1$) amplitudes to be crucial for the explosion of the $11.2\,M_\odot$ case because they obtained successful shock revival in 180-degree (pole-to-pole) simulations, whereas simulations with a 90-degree wedge around the equator did not explode.*). The violent shock motions and the associated shock expansion allow matter accreted through the shock to stay in the neutrino-heating region for a longer time. The increased abidance timescale in the gain layer enhances the efficiency of neutrino-energy transfer and thus supports the development of runaway conditions.

The shock-oscillation phenomenon exhibits strong similarity to the SASI dynamics that can be observed in 2D as well as 3D simulations of adiabatic accretion flows using an ideal-gas EoS and simple representations of the effects of neutrino cooling as regulator of (quasi-)stationary postshock conditions.[25),64),65)] An experimental shallow-water analog that considers a hydraulic jump in a converging two-

*) Successful shock revial, however, could also be obtained for the $11.2\,M_\odot$ star with a 90-degree pole-to-equator grid.

dimensional water flow has also been developed[66] to demonstrate the basic aspects of the instability that preferentially leads to low-order (dipolar, quadrupolar) shock deformation and violent, nonradial shock expansion and contraction. While the axis of these motions naturally coincides with the artificial symmetry (polar-grid) axis in 2D-axisymmetric simulations, there is no such predetermining constraint in the experimental setup. This confirms that the grid geometry is not the crucial aspect that allows the SASI sloshing phenomenon to occur. Moreover, the growth behavior of the SASI from the linear regime to the nonlinear stage in competition with neutrino-driven convective instability was investigated for supernova core conditions in 2D by Foglizzo et al. and Scheck et al. in Refs. 26), 63)[*]. In the linear regime both instabilities can be discriminated by their different growth behavior (oscillatory vs. nonoscillatory) and by the absence or presence of buoyant flow structures in the postshock shell. Stronger neutrino heating or slower advection velocities in the accretion flow were recognized to be favorable for the growth of neutrino-driven convection, whereas for insufficient heating and in fast accretion flows the SASI modes were seen to grow predominantly. Convective activity can also win when its growth is accelerated by strong buoyancy forces acting on large initial entropy perturbations. In the fully nonlinear regime, however, a clear separation of both instabilities could not be achieved and is very difficult, because SASI shock motions trigger secondary convection,[26] and inversely, it is also conceivable that neutrino-driven convection feeds back into enhanced SASI activity. Fundamental aspects of these hydrodynamical results seem to be in agreement with global linear stability analysis of stalled shocks in accretion flows (using a microphysical EoS and taking neutrino reactions into account) by Yamasaki & Yamada,[68] who found the dominant growth of oscillatory or nonoscillatory radial and nonradial modes, depending on the size of the imposed neutrino luminosities.

For all these reasons Marek & Janka[15] (see also Ref. 13)) interpreted the violent shock-sloshing motions with growing amplitudes, which preceded the explosions they found in $11.2\,M_\odot$ and $15\,M_\odot$ simulations, as a consequence of SASI activity. They were, however, fully aware that this was a speculative interpretation, a working hypothesis, which was by no means based on unambiguous facts and well-founded theoretical arguments. A solid theoretical foundation was (and still is) lacking for the nonlinear stage of the observed phenomenon. Nevertheless, it is clear that the energy input for the explosion has to be delivered by neutrino heating (whose behavior was quantitatively analysed and energetically evaluated by Marek & Janka), and that the shock oscillation motions are only helpful for improving the heating conditions, but by themselves are *not* the driving agency of the explosion. In this context it should be kept in mind that the growth of the SASI depends on an advective-acoustic cycle.[67] Once shock expansion initiates mass expansion behind the shock as well, the cycle tends to lose its support because the inward flow of matter is decelerated, diminished, or even quenched. It therefore seems unlikely that SASI is the dominant

[*] Numerous analytical and numerical studies for the linear growth regime of the SASI in supernova core like environments been performed. For probably the most comprehensive discussion including relevant references, see Ref. 67).

mode of nonradial mass motions up to the stage where the explosion takes off. It may, however, play a supportive role for establishing favorable neutrino-heating conditions and for getting close to the final runaway situation.

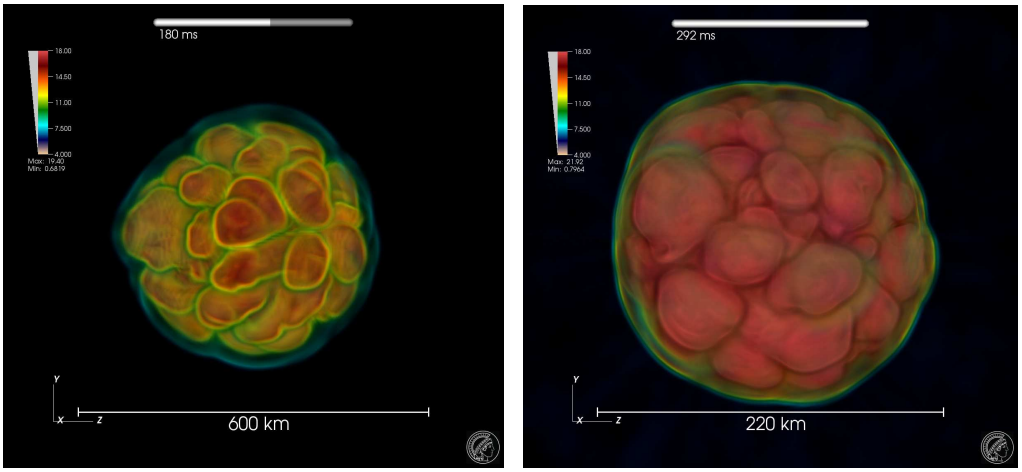

Fig. 20. Volume-rendering images of two instants (180 ms and 292 ms post bounce) of a first explorative 3D simulation of an 11.2 $M_\odot$ progenitor (model s11.2 of Ref. 40)) with full energy-dependent ray-by-ray three-flavor neutrino transport and the sophisticated set of neutrino opacities as applied also in the 1D and 2D models of the Garching group shown in Figs. 5–7 and 9–15. Neutrino-heated bubbles dominate the asymmetries in the postshock layer. The absence of large-amplitude bipolar SASI shock motions in this simulation challenges speculations in the literature[35] that local neutrino heating computed with the ray-by-ray approximation might unphysically correlate with low-order mode shock and matter motions and could be pumping them unphysically.

Burrows[35] classified the SASI as a "myth that has crept into modern discourse". (In fact, it has sneaked into his own works, too, cf., e.g., Refs. 53), 69).) In his view the vigorous dipolar shock oscillations seen in 2D simulations with full neutrino transport have been incorrectly associated with the SASI sloshing motions observed in simplified, neutrino-free studies. He argued that due to the inverse energy cascade of 2D turbulence, which transports energy from small to large scales, neutrino-heated, buoyant bubble convection with dominant low-ℓ modes has been confused with the SASI, whose growth rates are highest on the largest angular scales (i.e., for the spherical harmonics modes of lowest order $\ell \geq 1$). Such a possibility cannot be rejected categorically, it is indeed a viable possibility. Just as neutrino energy input might play a role as driving force of enhanced SASI activity, neutrino-driven buoyancy could also play a destructive role by destroying the flow coherence needed for SASI amplification.

But a proof of a negative feedback of neutrino-driven convection on the SASI has so far not been given, and a convincing demonstration of an exclusive dominance of neutrino-triggered buoyancy has also not been provided. Burrows et al.,[70] for example, argued that in their two-dimensional numerical toy model stronger neutrino heating and thus enhanced neutrino-driven convection was the cause of the growth of the dipolar sloshing amplitude that was crucial for getting neutrino-driven explo-

sions. This result, however, may be tightly connected to the simplified setup chosen for their simulations, especially with respect to the treatment of the neutrino source terms, by which energy losses from the cooling layer near the neutron star surface were massively underestimated. Moreover, neutrino emission from the neutron star interior was ignored and therefore the contraction of the neutron star was also underestimated. Investigations based on such very particular conditions without varying the progenitor structure, neutron star mass, gravity, and contaction behavior, as well as the efficiency of neutrino cooling, are endangered to lead to conclusions that hold for this special case but do not necessarily possess wider validity.

In consequence of the mentioned deficiencies of the neutrino and neutron star treatment, the accretion velocities are reduced, which implies more favorable conditions for the growth of neutrino-driven buoyancy while at the same time a possible importance of the SASI is suppressed, because the SASI is amplified more rapidly for shorter advection timescales in faster accretion flows (see, e.g., Ref. 26)). It is therefore not astonishing that Burrows et al.[70] observed only small SASI amplitudes in the absence of neutrino heating and the associated buoyant convection. It is also little astonishing that Murphy et al.[71] (also Ref. 72)) diagnosed the conditions in the same simplified modeling setup as fully consistent with neutrino-driven convection and turbulence in 2D as well as 3D simulations. The $27\,M_\odot$ calculation discussed above and in Sect. 3, which includes a sophisticated and self-consistent treatment of all relevant physics aspects, demonstrates that there are situations in collapsing stellar cores —at least under the constraint of axisymmetry and most obvious in the $25\,M_\odot$ and $27\,M_\odot$ cases— where the SASI is the most quickly growing instability and initially drives the shock expansion. It thus establishes, of course, also better conditions for enhanced neutrino heating. This may at some point change the situation from SASI-dominated to buoyancy-dominated, because it is clear that increasingly stronger neutrino heating will foster stronger buoyancy and thus will have a feedback on the flow dynamics (as already discussed in Ref. 26)). It is because of this interdependence of both instabilities that a dogmatic discussion about a dominant role of either the one or the other at all times and for all conditions seems counterproductive and meaningless.

A more serious possible argument against an important role of the SASI in real supernova cores at any time follows from the fact that all current 3D simulations that account for neutrino heating and cooling (Fig. 20; Refs. 18),23),24),31),34),55),70),73),74)) do not show the development of large-amplitude dipolar shock oscillations as seen in 2D models. Even for the $27\,M_\odot$ progenitor Ott et al.[75] could not find any strong evidence of SASI activity once neutrino-driven convection has started (whose fast growth, according to the authors, is enabled by sizable numerical perturbations caused by the employed cartesian grid).

Smaller saturation amplitudes of low-order shock oscillation modes in 3D have been explained by the distribution of turbulent kinetic energy over a larger number of available modes associated with the additional spatial degree of freedom in 3D compared to 2D.[73] This interpretation may be consistent with the observation that the direction of the dipolar deformation wanders stochastically[70] in 3D whereas its axis is artificially fixed to the polar symmetry axis in 2D models. Nevertheless,

the explanation is neither fully satisfactory nor generally valid, because it implicitly assumes that the total kinetic energy stored in turbulent flows of the gas in the postshock layer, in particular also in flow structures on the largest possible scales, cannot become considerably higher in 3D than in 2D. A priori a justification of this assumption is not obvious, but for some reason higher kinetic energies of the postshock layer indeed seem to be disfavored as suggested by the results in Ref. 24), which showed roughly the same nonradial kinetic energies in 2D and 3D models near the explosion.

Although current 3D simulations are still handicapped by a large number of approximations in the employed microphysics and neutrino transport, and although they mostly study highly simplified, parametrized setups[18),23),24),70)] or suffer from very limited numerical resolution[74)] or artificial, grid-induced perturbations[18),70),75)] (or even other, so far not realized, numerical problems in codes newly applied to the stellar core-collapse problem), the basic similarities of the outcome of the increasing pool of simulations lends growing support to expectations that SASI is subdominant in 3D.[35)] Instead, neutrino heating and associated buoyancy appear to be the main trigger of turbulent mass motions in the postshock layer and of the shock deformation seen in the numerical models.

Reflecting current results of 2D and 3D simulations, the conclusion seems to be unavoidable that the turbulent dynamics of the postshock mass motions in 3D is different from 2D and that this is likely to also affect the way how the nonradial flows in the neutrino-heating layer exactly foster the transition of the accretion shock to runaway expansion. If fully self-consistent, more sophisticated, well resolved, and not artificially grid-perturbed 3D models will confirm the current results of simplified, incomplete, deficient, and parametrized 3D setups, in which various feedback effects are ignored, we will be ready to agree with Dolence et al.[18)] that the supernova mechanism in 3D operates differently from 2D. It may be expected that the basic features and implications of 3D turbulence as seen in current models will be retained even in more elaborate simulations (unless the numerical grid of the simulations has a nonneglibile influence). It is less clear, however, whether the quasi-stationary shock expansion, which is less time-variable and less dynamic than in the 2D models, will survive when all relevant feedback effects are taken into account.

In any case, however, we do not think that these aspects imply a fundamental revision of the overall scenario of how core-collapse supernovae achieve to explode. In the end they only mean refinements in details, although, unquestionably, such refinements could be quantitatively relevant and even crucial. Nobody has rejected and can seriously deny the important role of neutrino-driven convection also in 2D. Independent of whether or not SASI has a supplementing function in 2D, whereas potentially being of reduced or minor relevance in 3D, the basic combination and interplay of ingredients in a working supernova mechanism will be same: Multi-dimensional hydrodynamic instabilities help pushing the shock to larger radii, thus stretching the dwell time of shock-accreted matter in the gain layer and enhancing the efficiency of neutrino-energy transfer. In the case of successful explosions, bubbles and large-scale plumes of neutrino-heated matter will rise (whether constrained by axisymmetry or not) to ultimately bring the shock up to the runaway threshold. The

mechanism is powered by neutrino-energy deposition, which also provides the energy input to the blast wave for unbinding the stellar envelope. The functioning of this neutrino-driven mechanism is crucially supported by hydrodynamic instabilities.

Not each and every single dynamical aspect that needs revision or receives refinement in the generalization from 2D to 3D modeling —as important for a precise and quantitative understanding it may be— will mean a fundamentally new twist of this basic picture of the mechanism. As an example in this context we mention the discussion of the runaway growth of buoyant, neutrino-heating-driven bubbles by Dolence et al.[18] The elements of this picture are not generically linked to the 3D situation (nor is this so for the discussion of the simplified, analytic toy model presented in the paper), they also apply to 2D geometry, and the basic outcome of the analysis concerning shock evolution as function of time as well as critical luminosity condition remind one of similar results for the 1D case (apart from a quantitative reduction of the threshold value of the critical luminosity by multi-dimensional effects).

§6. Summary and conclusions

We have discussed results of 2D simulations of the Garching group, in which for a growing set of progenitor stars successful, albeit mostly weak, neutrino-driven explosions could be obtained (Sects. 3 and 4). Most of these simulations were performed with a fully relativistic treatment and some with an approximate description of relativistic effects, but all of them included in a consistent manner the effects of hydrodynamics and of sophisticated, energy-dependent neutrino transport (either with ray-by-ray approximation or two-dimensional, two-moment closure). Despite interesting and quantitatively relevant differences in many details, the successful runs with relativistic physics are basically compatible with the simulations of the same progenitors with relativistic approximations.

We also attempted an assessment of these 2D results in the context of the current dispute about the dimensional dependence of the hydrodynamics of core-collapse supernovae (Sect. 5). Since 3D fluid dynamics in the supernova core seems to differ from 2D flows in a variety of aspects, what can one learn from self-consistently exploding 2D models? What can 2D modeling tell us at all, in particular since the explosions turn out to be weak and not to be able to reproduce observed supernova energies?

First, the 2D simulations show that multi-dimensional effects in the most sophisticated neutrino-hydrodynamics supernova models indeed lift the core conditions very close to the critical threshold for explosions, in most of the cases explored in Sect. 4 even beyond. This is obviously different from 1D modeling, where failures are obtained for all but the lowest-mass supernova progenitors. We therefore consider the 2D successes as quickening progress and as an excellent reason to appreciate the glass of wine —measuring our understanding of the supernova mechanism— as half full. Moreover, the successful explosions in 2D are certainly a very important and necessary confirmation of the notion that the critical luminosity needed for runaway conditions is reduced in the multi-dimensional case. A confirmation by sophisticated and fully self-consistent models was unquestionably necessary, because all other an-

alytical and numerical studies that reached this conclusion were done with highly idealized setups, in which most of the complex feedback processes in real supernova-core environments, especially also dissipative effects, were ignored.[9),10),14),23),24)]

Second, one should keep in mind that the neutrino-driven mechanism is powered by neutrino heating, which therefore is the crucial ingredient. Hydrodynamic instabilities, as indispensable as they may be, play "only" a supportive role. Although the exact way they operate is, of course, important for our theoretical understanding and demands detailed explorations, dimension-dependent differences like the question whether SASI plus neutrino-driven convection or mere neutrino-driven convection and 3D turbulence are the assisting agencies of shock expansion, are possibly more a kind of refinement than an aspect of central nature in the fundamental problem of the explosion mechanism. Despite the constraint to two dimensions, successfully exploding models therefore lend strong support to the viability of the neutrino-driven mechanism.

The recent literature on the explosion mechanism in different dimensions contains a variety of incorrect claims. One of them, for example, is the argument that local neutrino heating associated with ray-by-ray neutrino transport unphysically correlates with low-order mode shock and matter motions and unphysically pumps them.[35)] Generally, however, a problem of this kind appears highly unlikely because violent, bipolar motions of the shock and postshock layer were seen in 2D models with ray-by-ray transport as well as with true 2D transport schemes (cf. Fig. 17 and, e.g., Refs. 53),54),69)) and even with simple neutrino-heating terms based on a spherical neutrino-lightbulb description (e.g., Refs. 14),23),24)). Moreover, vigorous sloshing motions of the shock were neither found for all investigated progenitors in 2D simulations (see Fig. 10) nor were they obtained in 3D models with ray-by-ray neutrino treatment (Fig. 20), although such shock dynamics was present in 2D. Ray-by-ray transport and large-amplitude SASI sloshing of the shock therefore do not seem to have any tight causal connection. Another incorrect claim concerns an alleged proposition by Hanke et al.[24)] that 3D simulations exhibit the tendency to become more similar to 1D results. Hanke et al. reported their observations and partly speculative interpretation of results for a very specific, highly artificial and simplified modeling setup adopted from other works for comparison, in which they found less readiness for explosions in 3D simulations with increasing grid resolution. This result is still not understood in a broader context, but in the unsuccessful 3D cases the shock evolution and some, but not all, explosion-relevant quantities (naturally and undisputably) became more similar to 1D simulations, and the postshock flow showed less vigorous mass motions than in the corresponding, successful 2D models. The statement by Hanke et al. was therefore made in reference to these special results but was not meant to be a prediction for 3D supernova dynamics in general.

Current simulations in different dimensions suggest interesting possible differences of the flow dynamics in supernova cores between 1D, 2D, and 3D. In (artifically exploded) 1D models the transition from shock stagnation and accretion to runaway shock expansion takes place either through a number of radial shock pulsations or by a continuous growth of the shock radius until accelerating expansion sets in.[5),10)]

While self-consistent 1D simulations do not produce explosions, 2D models show a reduced neutrino-luminosity threshold for the onset of explosions. In this case violent, nonradial shock oscillations (potentially connected to SASI activity) with increasing amplitude are seen for many but not for all progenitors. The conditions in the progenitor seem to play a crucial role for the type of observed behavior. More violent shock oscillations appear to occur in more massive stars with compact cores. Less massive progenitors with their less compact cores and faster decay of the mass accretion rate exhibit more signs of classical neutrino-driven buoyancy, in which case the shock expansion is more spherical and more continuous. In 3D, at least as far as current models of different sophistication —but only few with self-consistent coupling of hydrodynamics and neutrino transport,[31),34),55),74),75)] and all of them still with many simplications and deficiencies— allow one to conclude, the shock expansion appears to be more quasi-stationary, driven by the inflation of neutrino-heated bubbles. The turbulent fragmentation of these bubbles leads to potentially large shock deformation but seems to push the shock outward in all directions more continuously than in 2D.

While the first 3D results are inspiring and show new possible twists and directions in the interplay of different physical ingredients of the highly complex problem of the supernova explosion mechanism, these first 3D simulations leave more open questions than they can answer. While general agreement exists about the supportive influence of multi-dimensional postshock flows in 2D, present results are inconclusive whether there is a further reduction of the critical luminosity in 3D compared to 2D. The results of Hanke et al.[24)] are in conflict with corresponding claims by Nordhaus et al.,[23)] and the more recent results of the Princeton group[18),70)] also show a considerable weakening of the effect advocated previously: Although the newest 3D simulations of the Princeton group still yield somewhat earlier ($\sim$100–200 ms) explosions than their 2D models, the critical luminosity differences found before have nearly disappeared. A general trend to faster explosions in 3D, however, is neither clearly supported by the results of Ref. 24) nor by the outcome of more sophisticated models by L. Scheck.[76)] So does 3D turbulence foster the onset of explosions even better than 2D flows? And if so, how large is the difference and by which effects is it caused? Turbulence in 3D pumps energy into smaller scales, but the energy stored on these scales is much lower than that on large scales. How can this have a considerable, supportive influence on the shock revival? Only a smaller fraction of the fluid elements (tracer particles) in 3D simulations[18),74)] is found to possess longer dwell times in the gain layer, but a significantly larger fraction has shorter ones than in 2D, which is fully compatible with the longer neutrino-heating timescales and lower net heating rates seen in 3D. If it is not more efficient neutrino heating, which 3D effects could account for faster explosions than in 2D models? Is it possible that different dimension-dependent effects in opposite directions compete with each other and partially compensate each other, which might explain seemingly contradictory trends of 2D vs. 3D found by different groups? Conclusive answers have not been given yet. In view of the turbulent energy cascade, are vigorous low-order modes of postshock mass motions generally excluded in 3D? Does neutrino-driven convection possibly destroy the coherence of SASI sloshing and spiral modes? Does SASI play

a role at all in supernova cores or are all relevant mass motions in 2D and 3D pure neutrino-driven convection as hypothesized in Ref. 35). Again, conclusive answers do not exist. If 3D turbulence on small scales is the crucial phenomenon that discriminates the onset of explosions in 3D from those in 2D, what is the influence of numerical resolution, what are the consequences of different grid treatments (spherical vs. cartesian, adaptive meshes vs. fixed ones) and of different hydro solvers? And, on the level of physics, what is the influence of neutrino viscosity and in particular of magnetic viscosity? If small-scale turbulence is relevant, the amplification of the fields may not be negligible and may have an influence on the dissipation scale and on the transport of energy.

In order to receive reliable answers, self-consistent models with all relevant ingredients will be needed. Not every simplified approach that may be sufficient for studying observable consequences and measurable signals connected to supernova explosions initiated by the neutrino-driven mechanism, is equally justified when the explosion mechanism itself and its determining factors are to be explored. The lack of self-consistency and of important feedback effects may produce misleading results where subdominant effects show up much more strongly than they would if all relevant physics were included. In order to reliably account for the feedback of neutrino transport, generic transport effects have to be included and sufficient resolution is indispensable, in particular also in the surface-near neutron star layers where the density gradient steepens with time and the accretion-regulating cooling region is squeezed into a narrow shell with tremendously increasing cooling rates per nucleon (in Ref. 5) the cooling rates at late postbounce times were at least 10 times higher than those shown in Ref. 18)!). Also numerical artifacts potentially caused by grid effects and grid perturbations or numerical diffusion, e.g. connected to adaptive mesh refinement, will have to be investigated. Finally, if different hydrodynamic instabilities compete in their growth, the results might not be independent of the initial seed perturbations, and the still unsettled variations of physical quantities in the convective regions of the progenitor cores might predetermine the growth of the instabilities after core bounce.[75),77)] Not only is a reliable definition of these initial conditions needed; also (noise-free) dynamical simulation codes that allow for a tracking of the growth behavior of these initial asymmetries during infall and postbounce evolution, will be necessary.

Supernova modelers have only now begun to touch the vast wealth of dynamical phenomena that may play a role in the explosion mechanism of neutrino-heated supernova cores in the third dimension. Astonishing discoveries may be waiting for us when we continue to move forward into this unexplored territory. Don't let us freeze in humility in the face of this age-old challenge but let us get down to work! A lot of fun will be our reward!

Acknowledgements

We thank Elena Erastova and Markus Rampp (Max-Planck-Rechenzentrum Garching) for their help in the visualization of our 3D data in Fig. 20. Data from simulations by the Garching group are accessible either openly or upon request at

`http://www.mpa-garching.mpg.de/ccsnarchive/`. This work was supported by Deutsche Forschungsgemeinschaft through grants SFB/TR7 "Gravitational-Wave Astronomy" and EXC 153 "Cluster of Excellence: Origin and Structure of the Universe". M.O. is grateful for support from the European Research Council (grant CAMAP-259276). We acknowledge that results in this paper have been achieved using the PRACE (Tier-0) Research Infrastructure resources CURIE (France/CEA) and SuperMUC (Germany/LRZ). Moreover, HPC resources (Tier-1) at the NIC/Jülich through a PRACE-2IP/DECI-7 grant are acknowledged.

References

1) Stuart L. Shapiro and Saul A. Teukolsky, *Black Holes, White Dwarfs, and Neutron Stars* (John Wiley & Sons, New York, 1983).
2) H.-Th. Janka, Annu. Rev. Nucl. Part. Sci. **62** (2012), 407.
3) M. Th. Keil, G. Raffelt and H.-Th. Janka, Astrophys. J. **590** (2003), 971.
4) M. Rampp and H.-Th. Janka, Astron. Astrophys. **396** (2002), 361.
5) R. Buras, M. Rampp, H.-Th. Janka and K. Kifonidis, Astron. Astrophys. **447** (2006), 1049.
6) B. Müller, H.-Th. Janka and H. Dimmelmeier, Astrophys. J. Suppl. **189** (2010), 104.
7) H. A. Bethe and J. R. Wilson, Astrophys. J. **295** (1985), 14.
8) H.-Th. Janka, Astron. Astrophys. **368** (2001), 527.
9) A. Burrows and J. Goshy, Astrophys. J. **416** (1993), L75.
10) R. Fernández, Astrophys. J. **749** (2012), 142.
11) H.-Th. Janka and W. Keil, astro-ph/9709012.
H.-Th. Janka, K. Kifonidis and M. Rampp, in *Physics of Neutron Star Interiors* (Springer,Berlin,2001), p.333.
12) T. A. Thompson, E. Quataert and A. Burrows, Astrophys. J. **620** (2005), 861.
13) R. Buras, H.-Th. Janka, M. Rampp and K. Kifonidis, Astron. Astrophys. **457** (2006), 281.
14) J. W. Murphy and A. Burrows, Astrophys. J. **688** (2008), 1159.
15) A. Marek and H.-Th. Janka, Astrophys. J. **694** (2009), 664.
16) B. Müller, H.-Th. Janka and A. Marek, Astrophys. J. **756** (2012), 84.
17) B. Müller, H.-Th. Janka and A. Heger, Astrophys. J., in press, arXiv:1205.7078.
18) J. C. Dolence, A. Burrows, J. W. Murphy and J. Nordhaus, arXiv:1210.5241.
19) M. Herant, W. Benz, W. R. Hix, C. L. Fryer and S. A. Colgate, Astrophys. J. **435** (1994), 339.
20) A. Burrows, J. Hayes and B. A. Fryxell, Astrophys. J. **450** (1995), 830.
21) H.-Th. Janka and E. Müller, Astron. Astrophys. **306** (1994), 167.
22) T. Yamasaki and S. Yamada, Astrophys. J. **650** (2006), 291.
23) J. Nordhaus, A. Burrows, A. Almgren and J. Bell, Astrophys. J. **720** (2010), 694.
24) F. Hanke, A. Marek, B. Müller and H.-Th. Janka, Astrophys. J. **755** (2012), 138.
25) J. M. Blondin, A. Mezzacappa and C. DeMarino, Astrophys. J. **584** (2003), 971.
26) L. Scheck, H.-Th. Janka, T. Foglizzo and K. Kifonidis, Astron. Astrophys. **477** (2008), 931.
27) A. Arcones and F.-K. Thielemann, arXiv:1207.2527.
28) I. Tamborra, G. G. Raffelt, L. Hüdepohl and H.-Th. Janka, JCAP **01** (2012), 013.
29) L. Scheck, K. Kifonidis, H.-Th. Janka and E. Müller, Astron. Astrophys. **457** (2006), 963.
30) M. Ugliano, H.-Th. Janka, A. Marek and A. Arcones, Astrophys. J. **757** (2012), 69.
31) A. Wongwathanarat, H.-Th. Janka and E. Müller, Astrophys. J. **725** (2010), L106.
32) J. Nordhaus, T. D. Brandt, A. Burrows, E. Livne and C. D. Ott, Phys. Rev. D **82** (2010), 103016.
33) J. Nordhaus, T. D. Brandt, A. Burrows and A. Almgren, Mon. Not. Royal Astron. Soc. **423** (2012), 1805.
34) A. Wongwathanarat, H.-Th. Janka and E. Müller, arXiv:1210.8148.
35) A. Burrows, arXiv:1210.4921.
36) K. Nomoto, Astrophys. J. **277** (1984), 791.
K. Nomoto, Astrophys. J. **322** (1987), 206.

37) F. S. Kitaura, H.-Th. Janka and W. Hillebrandt, Astron. Astrophys. **450** (2006), 345.
38) H.-Th. Janka, B. Müller, F. S. Kitaura and R. Buras, Astron. Astrophys. **485** (2008), 199.
39) S. Wanajo, H.-Th. Janka and B. Müller, Astrophys. J. **726** (2011), L15.
40) S. E. Woosley, A. Heger and T. A. Weaver, Rev. Mod. Physics **74** (2002), 1015.
41) H. Shen, H. Toki, K. Oyamatsu and K. Sumiyoshi, Nucl. Phys. A **637** (1998), 435.
42) J. Lattimer and F. Swesty, Nucl. Phys. A **535** (1991), 331.
43) A. Marek, *Multi-Dimensional Simulations of Core-Collapse Supernovae with Different Equations of State for Hot Proto-Neutron Stars* (PhD Thesis, TU München, 2007).
44) B. Müller, H.-Th. Janka and A. Marek, arXiv:1210.6984.
45) L. Dessart, A. Burrows, E. Livne and C. D. Ott, Astrophys. J. **645** (2006), 534.
46) S. E. Woosley and T. A. Weaver, Astrophys. J. **101** (1995), 181.
47) E. O'Connor and C. D. Ott, arXiv:1207.1100.
48) M. Liebendörfer, M. Rampp, H.-Th. Janka and A. Mezzacappa, Astrophys. J. **620** (2005), 840.
49) A. Marek, H. Dimmelmeier, H.-Th. Janka, E. Müller and R. Buras, Astron. Astrophys. **445** (2006), 273.
50) M. Kachelrieß, R. Tomàs. R. Buras, H.-Th. Janka, A. Marek and M. Rampp, Phys. Rev. D **71** (2005), 063003.
51) E. O'Connor and C. D. Ott, Astrophys. J. **730** (2011), 70.
52) A. Marek, H.-Th. Janka and E. Müller, Astron. Astrophys. **496** (2009), 475.
53) C. D. Ott, A. Burrows, L. Dessart and E. Livne, Astrophys. J. **685** (2008), 1069.
54) T. D. Brandt, A. Burrows, C. D. Ott and E. Livne, Astrophys. J. **728** (2011), 8.
55) E. Müller, H.-Th. Janka and A. Wongwathanarat, Astron. Astrophys. **537** (2012), A63.
56) A. Heger, private communication (2011).
57) D. L. Meier, R. I. Epstein, W. D. Arnett and D. N. Schramm, Astrophys. J. **204** (1976), 869.
58) S. Akiyama, J. C. Wheeler, D. L. Meier and I. Lichtenstadt, Astrophys. J. **584** (2003), 954.
59) A. Heger, S. E. Woosley and H. C. Spruit, Astrophys. J. **626** (2005), 350.
60) M. Obergaulinger and H.-Th. Janka, arXiv:1101.1198.
61) E. Endeve, C. Y. Cardall, R. D. Budiardja and A. Mezzacappa, Astrophys. J. **713** (2010), 1219.
62) E. Endeve, et al., Astrophys. J. **751** (2012), 26.
63) T. Foglizzo, L. Scheck and H.-Th. Janka, Astrophys. J. **652** (2006), 1436.
64) J. M. Blondin and A. Mezzacappa, Nature **445** (2007), 58.
65) R. Fernández, Astrophys. J. **725** (2010), 1563.
66) T. Foglizzo, F. Masset, J. Guilet and G. Durand, Phys. Rev. Lett. **108** (2012), 051103.
67) J. Guilet and T. Foglizzo, Mon. Not. Royal Astron. Soc. **421** (2012), 546.
68) T. Yamasaki and S. Yamada, Astrophys. J. **656** (2007), 1019.
69) A. Burrows, E. Livne, L. Dessart, C. D. Ott and J. Murphy, Astrophys. J. **655** (2007), 416.
70) A. Burrows, J. C. Dolence and J. W. Murphy, Astrophys. J. **759** (2012), 5.
71) J. W. Murphy, J. C. Dolence and A. Burrows, arXiv:1205.3491.
72) J. W. Murphy and C. Meakin, Astrophys. J. **742** (2011), 74.
73) W. Iwakami, K. Kotake, N. Ohnishi, S. Yamada and K. Sawada, Astrophys. J. **678** (2008), 1207.
74) T. Takiwaki, K. Kotake and Y. Suwa, Astrophys. J. **749** (2012), 98.
75) C. D. Ott, et al., arXiv:1210.6674.
76) A. Marek, *Parametric Studies of Hydrodynamic Instabilities in the Supernova Core by Two- and Three-Dimensional Simulations* (PhD Thesis, TU München, 2006).
77) W. D. Arnett and C. Meakin, Astrophys. J. **733** (2011), 78.